SPECKLE REDUCTION FOR THE ENHANCEMENT OF ULTRASOUND IMAGES

A DISSERTATION

Submitted in partial fulfillment of the
requirements for the award of the degree
of
MASTER OF TECHNOLOGY
in
ELECTRICAL ENGINEERING
(With Specialization in Measurement & Instrumentation)

By
VIKAS GUPTA

DEPARTMENT OF ELECTRICAL ENGINEERING
INDIAN INSTITUTE OF TECHNOLOGY ROORKEE
ROORKEE - 247 667 (INDIA)
JUNE, 2008

I.D. No.-M.V 450 /2008-34 VK

CANDIDATE'S DECLARATION

I hereby declare that the work presented in this dissertation entitled **"SPECKLE REDUCTION FOR THE ENHANCEMENT OF ULTRASOUND IMAGES"** submitted in partial fulfillment of the requirements for the award of the Degree of **Master of Technology** in **Electrical Engineering** with specialization in **Measurement and Instrumentation**, in the Department of Electrical Engineering, **Indian Institute of Technology, Roorkee** is an authentic record of my own work carried out from June 2007 to June 2008 under the guidance and supervision of Dr. Vinod Kumar (Professor, Electrical Engineering Department, Indian Institute of Technology, Roorkee).

I have not submitted the matter embodied in this report for the award of any other degree or diploma.

Date: 30 June'08

Place: Roorkee

Vikas

(VIKAS GUPTA)

CERTIFICATE

This is to certify that the above statement made by the candidate is true to the best of my knowledge and belief.

Dr. Vinod Kumar
Professor
Electrical Engineering Department
Indian Institute of Technology, Roorkee
Roorkee-247667 (India)

ACKNOWLEDGEMENTS

I express my deepest sense of gratitude towards my guide Dr. Vinod Kumar, Professor, Department of Electrical Engineering of Indian Institute of Technology, Roorkee, for his patience, inspirational guidance, constant encouragement, moral support, and keen interest in the finest details of my work.

My special thanks to Lt. Col. Dr. M. R. Kural, Radiologist, M. D., CMO, IIT Roorkee Hospital & Dr. Manju Saini, M. D., Radiodiagnosist, HIHT, Dehradun, for their valuable help in evaluation of ultrasound images.

My heartfelt gratitude and indebtness goes to all the faculty members of Measurements and Instrumentation group who, with their encouraging and caring words, constructive criticism and suggestions have contributed directly or indirectly in a significant way towards completion of this thesis.

I am indebted to all my classmates from Measurements & Instrumentation group for taking interest in discussing my problems and encouraging me. Last but not least I would like to acknowledge my family members for their never fading love and support. I express my gratitude to all those who helped me directly or indirectly in the successful completion of my dissertation.

VIKAS GUPTA

ABSTRACT

Ultrasound imaging has been established as one of the most important techniques in the field of the medical diagnostic technology because of its non-invasing nature, portability, low cost and real time information. The image quality is of central importance in an ultrasound examination as the diagnosis of a disease by a radiologist is based on his interpretation of the medical images. However, ultrasound images suffer from an intrinsic artifact called speckle. Speckle degrades spatial and contrast resolution and obscures the underlying anatomy. It makes human interpretation and computer-assisted detection techniques difficult and inconsistent. Since speckle is a major shortcoming of ultrasound, reducing or eliminating speckle is necessary for the visual enhancement and auto segmentation improvement.

In this thesis work speckle reduction techniques have been implemented to increase the visualization and to make the auto segmentation process easy and fast in medical ultrasound images.

The adaptive filtering and anisotropic diffusion based techniques have been examined and compared on the basis of their speckle suppression ability and feature preservation. Under the adaptive filtering, adaptive weighted median filter (AWMF) and aggressive region growing filter (ARGF) have been implemented. Both algorithms uses local statistics of the image for the filtering action. AWMF is an enahnced median filter and it is based on weighted median. Aggressive region growing filter (ARGF) selects a filtering region size using an appropriately estimated homogeneity value for region growth. In case of diffusion based techniques speckle reduction anisotropic diffusion (SRAD) has been applied. SRAD is based on the same minimum mean square error (MMSE) approach to filtering as Lee and Kuan filters.

These filtering algorithms are applied on the simulated and the tissue mimicking phantom to have a quantitative analysis. To study the feasibility and usefulness of these methods, the algorithms are applied on the real ultrasound image taken from GE website and medpix database. To quantify the results obtained by these three techniques, evaluation indices (CNR, FOM, MSSIM) have been calculated.

It is found that SRAD is superior to adaptive filtering based techniques in increasing the visualization of the images while reducing the speckles. AWMF cannot remove the speckles effectively and also causes blurring with the loss of details. ARGF technique reduces the speckles effectively and its smoothening effect can be used as a preprocessing step for auto segmentation and image registration.
Qualitative analysis for these three methods has been done by the assistance of the medical experts. The results obtained may be useful for radiologists, clinicians or experts , who may use it for clinical diagnosis.

List of Figures

List of Tables

Contents

Chapter 1

Introduction

1.1 Medical Imaging: An Overview

Medical imaging is a technique which is used to provide images of the anatomy of the human body for the medical diagnosis. It is composed of set of techniques that create images of the internal structure of the body without affecting the functional processes occurring inside human body. Medical imaging at various level permit the detection and diagnosis of disease or the abnormality at an earlier stage.
Recent advances in the imaging technology have drastically changed the medical diagnosis. The imaging modalities such as X-ray, Computed Tomography (CT), Magnetic Resonance Imaging (MRI), Ultrasound and other modalities provide exceptional view of the internal anatomy, but the analysis of the embedded structures depend on the radiologists experience. In this context, the need for the computer assisted approaches has been felt by the medical image analysis community. In many radiological applications, the visualization and quantitative analysis of physiological structures provide valuable clinical information that is extremely useful for diagnosis and treatment. Using the sophisticated computer programs and model, the physiological structures can be processed and manipulated to reveal the diagnostic features that are difficult to observe in original image[1]. But it should not introduce artifacts in the images which can lead to a wrong interpretation.

1.2 Ultrasound Imaging

The main objective of a medical imaging is to acquire useful information about the physiological processes or organs of the body by using external or internal sources of energy. The choice for a particular medical imaging modality is governed by several factors such as resolution, contrast mechanism, convenience, safety and cost effective. The medical use of ultrasound has expanded enormously over the last two decades, due largely to the fact that it is safe, allows real-time visualization of moving structures, is suitable for many clinical applications, and is relatively inexpensive. The following subsections describe the basics of ultrasound imaging.

1.2.1 Principle Of Ultrasound Imaging

Ultrasound imaging is based on the 'pulse-echo' principle in which a beam of ultrasound is emitted from a transducer and directed into the tissue. The ultrasound machine transmits sound pulses into the body using a probe capable of generating and detecting the sound waves. When an ultrasound pulse sees an interface between soft tissues having different acoustic impedance, a small portion of the ultrasound beam is reflected but most passes across the interface undeviated. The fraction of these reflections that return to the direction of the incident ultrasound beam is called as backscattered signal.
When the sound waves hit a boundary between tissues (e.g. between fluid and soft tissue, soft tissue and bone) some of the sound waves are reflected back to the probe and the rest travel on further until they reach another boundary and are reflected back. The reflected waves are detected by the probe and relayed to the machine. The machine calculates the distance from the probe to the tissue or organ (boundaries) using the speed of sound in tissue (1,540 m/s) and the time of each echo's return . The machine displays the distances and intensities of the echoes on the screen and forms a two dimensional image.

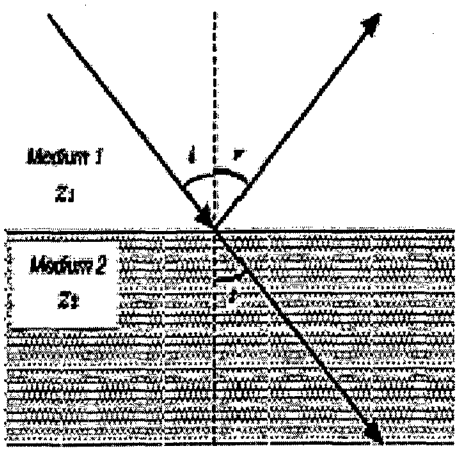

Figure 1.1: Reflection of ultrasound beam[2]

1.2.2 Ultrasound Imaging System

A simplified block diagram of an ultrasound system is shown in the figure 1.2. In this system there is a piezoelectric crystal based multi-element transducer at the end of a relatively long cable. In this type of system the operator is provided with various transducer probe heads to select for optical imaging.

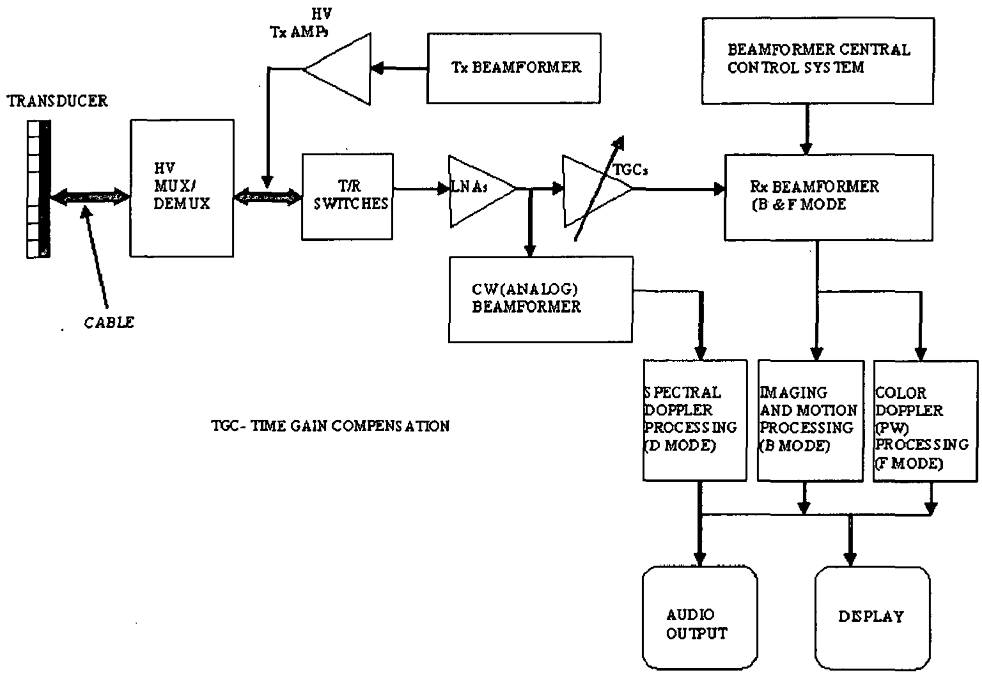

Figure 1.2: Ultrasound system block diagram [3]

The ultrasound system shown consists of electronic transmitter/receiver switching circuits, control panel with pulse generation and control, and computer processing and display system. There are three main ultrasonic acquisition modes: B-mode (gray-scale imaging; 2D); F-mode (Colorflow or Doppler Imaging; blood flow); and D-mode (Spectral Doppler). B-mode creates the traditional gray-scale image; F-mode is a color overlay on the B-mode display that shows blood flow; D-mode is the Doppler display that might show blood flow velocities and their frequencies. (There is also an M-mode, which displays a single B-mode time line.) In medical imaging the operating frequencies are in the range of 1 MHz to 40 MHz. Higher frequencies are in principle more desirable, since they provide higher resolution but tissue attenuation limits how high the frequency can be for a given penetration distance.

1.2.3 Medical Application Of Ultrasound

The medical use of ultrasound has expanded enormously over the last two decades, due largely to the fact that it is safe and inexpensive. The ultrasound imaging is applied for scanning soft tissues like lungs, liver, rectum, prostate, uterus, and neonatal brain. It is excellent for the measurement of flow and motion. Also 2D-real time scanning is possible and 3D, 4D techniques are evolving.

1.3 Speckle Reduction Review

Ultrasound speckle is a granular pattern formed by the constructive and destructive interference of the backscattering echoes from the scatterers smaller than the resolution size. This pattern occurs especially when an ultrasound scan of organs like liver and kidney is taken whose underlying structures are too small to be resolved by the ultrasound scanners. Speckle degrades the image quality in ultrasound B-scans and hence reduces the ability of human observer to discriminate the fine details in diagnostic examination[4]. It also decreases the efficiency of further image processing techniques such as edge detection, image segmentation or image registration . Therefore, speckle reduction is necessary for the enhancement of ultrasound images.

An examination of the literature shows a number of speckle reduction techniques. Various speckle reduction approaches are based on image post processing and image averaging or compounding. In averaging based approaches multiple decorrelated frames are averaged out. These decorrelated images are sampled at different times, from different views, or with different frequencies for the same target[5],[6]. Averaging techniques suffer from limited speckle reduction effects - speckle is reduced to $\sqrt{n}$ where n is the number of frames. Additionally, the multiple frames in averaging techniques reduce the frame rate, making the techniques of limited practical use.

On the other hand techniques based on post processing approaches involve non adaptive or adaptive filtering of B-scan images to smooth out the speckle. But non adaptive techniques causes severe blurring in the ultrasound images and are not able to preserve boundaries between the two regions with slightly different gray level. Adaptive filtering techniques have been developed for feature detection in ultrasound images. As with the median filtering, these techniques produces filter output at each pixel from the properties of the pixels inside region $W_{i,j}$ containing the pixel of interest. The adaptive weighted median filter (AWMF) [7] is an enhanced median filter. The weighted median of a region $W_{i,j}$ pixels is defined as the median of an extended sequence formed by replicating pixels in $W_{i,j}$ by an amount calculated from their distance to (i,j) and the estimate of the local statistics. The AWMF technique eliminates the requirement that speckle artifacts be smaller than the half the region size as is required for pure median filtering. Another scheme for filtering is also defined, where the adaptive speckle suppression filter (ASSF) is used for the smoothening of the images using local statistics [4]. The filter adaptation is achieved by using correct shape and size of the local filtering kernels. Each kernel is suitable for reducing the noise with an arbitrarily shaped homogenous region containing the processed pixel. These kernels are obtained through region growing approach, which uses local statistics of the image. Through implementation and analysis, it is found that the quality of the AWMF filtering technique is sensitive to the values of the empirically selected parameters used in algorithm. Also in ASSF filter, these parameters selection cause the region to grow too large and blur the important edges. An alternative approach for improving the speckle suppression is to expand the local processing region as much as possible, allowing non speckle pixel to dominate speckle pixels in population. Koo and Park [8] proposed a technique called homogenous region growing mean filter which required a prespecified, image dependent homogeneity as a threshold value. The local homogeneity is estimated initially with in an estimated window W_{ij} of default size containing the pixel (i,j). The ratio of pixel variance to pixel mean in the window is a typical estimator. If the initial seed region satisfies local homogeneity criteria it is taken as the seed region otherwise it is contracted until it satisfies the homogeneity criteria. Then the seed region is expanded till the maximum sized homogenous region is obtained. The output pixel is set to the mean intensity of this region.

Partial differential equation based methods have been widely used for image denoising with edge preservation. These methods are either based on the axiomatic approach of non linear scale space or on the variational approach of energy function minimization. The PDE based speckle reduction approach allows the generation of an image scale space (a set of filtered image that vary from fine to coarse level). The PDE based approaches not only preserves the edges but also enhance it by inhibiting diffusion across the edges but allowing diffusion on either side of the image. This approach is adaptive and does not use hard threshold to alter performance in homogenous region or in regions near the edges and small features [10, 11]. A partial differential equation (PDE) approach to speckle removal called speckle reducing anisotropic diffusion (SRAD) has been developed [10]. The diffusion technique is based on the same minimum mean square error (MMSE) approach to filtering as the Lee (Kuan) and Frost filters. In fact, SRAD can be related directly to the Lee and Frost window-based filters. So, SRAD is the edge sensitive extension of conventional adaptive speckle filter, in the same manner that the original Perona and Malik anisotropic diffusion [12] is the edge sensitive extension of the average filter. In this sense, it is the extension of application of anisotropic diffusion to medical ultrasound in which signal-dependent, spatially correlated multiplicative noise is present.

1.4 Objective of Thesis

Speckle degrades the image quality in ultrasound B-scans and hence reduces the ability of radiologists to discriminate the fine details in diagnostic examination. In such cases computer aided diagnosis (CAD) can provide a second opinion to radiologist's interpretation of medical images. This thesis works deals with the implementation of speckle reduction algorithms so as to improve the quality and productivity by improving the accuracy of radiological diagnosis and reducing the time taken in the manual analysis of the images. The main goal of this work is to reduce the speckles in the ultrasound images while retaining the fine details and diagnostic features. A proposed scheme has been shown in fig1.3. Since there is no standard speckle free image available, for the purpose of evaluating the performance of the filtering algorithms the speckles have been simulated using the Loupas' model and shape images are corrupted with simulated speckle to resemble the noisy image. Then the three algorithms (AWMF, ARGF and SRAD) are applied on the corrupted images and their results are quantified using the quantitative indices. Finally based on the comparison, the best filtering algorithm is found in terms of its speckle reduction ability and feature preservation. These algorithms are applied on the real ultrasound images to study their feasibility and usefulness. Qualitative analysis will be done by radiologists.

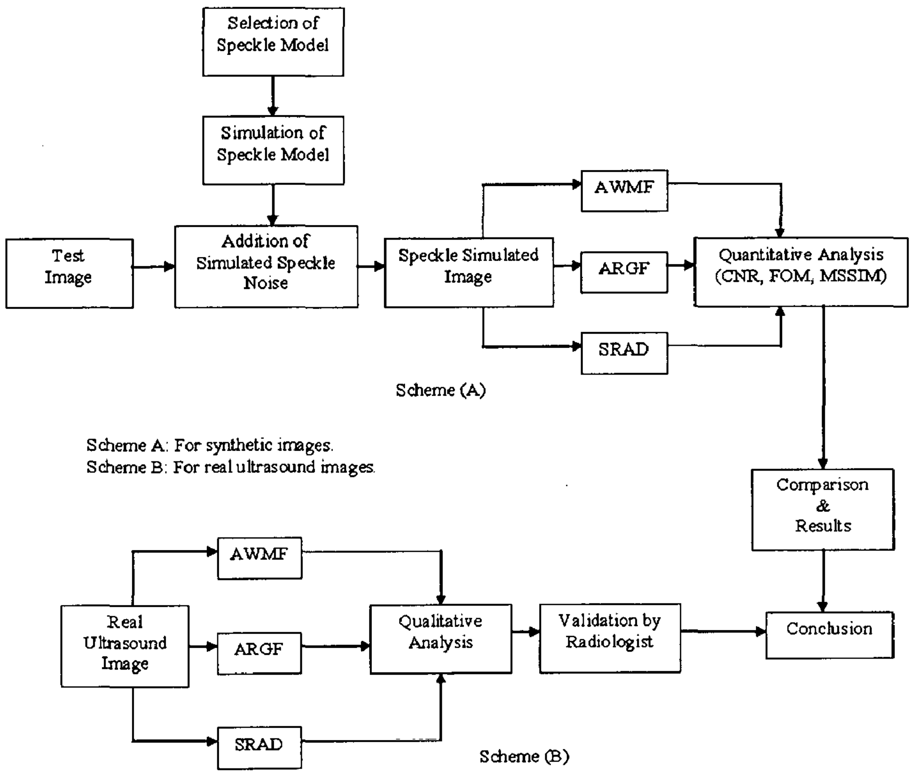

Figure 1.3: Block diagram for proposed scheme

1.5 Organisation of Thesis

The present thesis work is organized as follows:
Chapter1 introduces the basics of the ultrasound imaging and their application in the medical diagnosis. A brief review of the speckle reduction techniques has also been given. In chapter 2 the origin of speckle and the various speckle models have been discussed to understand their statistics. A brief description of the adaptive based filtering techniques has been given in chapter 3. Under this the two adaptive

filters AWMF and ARGF have been implemented and an analysis of their result has been done.Chapter 4 describes the anisotropic diffusion filtering for speckle reduction in the ultrasound images. A diffusion based technique called speckle reduction anisotropic diffusion has been examined in this chapter. In chapter 5 the results of the comparative analysis of the filtering efficiency and feature preservation capability of the three algorithms have been given. The evaluation criteria is based on the quantitative indices (CNR, FOM, MSSIM). Chapter 6 finally presents the conclusions and the possible directions for further work. The references cited in the thesis are enlisted at the end.

Chapter 2

Speckle Analysis

2.1 Introduction

This chapter gives the brief description about the origin of speckles in the ultrasound images and the various models to understand their statistics. The nature of speckle has been a major subject of investigation. The most commonly used model to explain the effects that occur when a tissue is insonified, as shown in Figure 2.1. As shown a tissue is modelled as a sound absorbing medium containing "scatterers" which scatter the sound waves. These scatterers arise from structures approximately equal to or smaller in size than the wavelength of the ultrasound. In other words, they result from the tissue microstructure (like microvasculature, cell conglomerates etc.).

Ultrasound B-scan images represent the back-scattering of an ultrasound beam from structures inside the body. There are two main types of scattering: diffuse scattering which leads to speckle in the image, and coherent scattering that creates clear light and dark features. Diffuse scattering arises when there are a large number of scatterers with random phase within the resolution cell of the ultrasound beam. Coherent scattering results when the scatterers in the resolution cell are in phase. The diffuse scatterers are assumed to be uniformly distributed over space. This random nature of the location of the scatterers results in speckle pattern and changes their statistical nature. Consequently, a statistical approach to its analysis should be done.

While analyzing speckle it is to be noted that the speckle as appearing in the image are different from those in the RF envelope.The RF signal is subjected to several transformations on its way from the transducer to the screen that affects its statistics. The most important of these is the log compression of the signal, used to reduce the dynamic range of the input echo signal to match the lower dynamic range of the display device. The input signal could have dynamic ranges of the order 50-70 dB whereas a typical display have a dynamic range of the order of 20-30 dB.

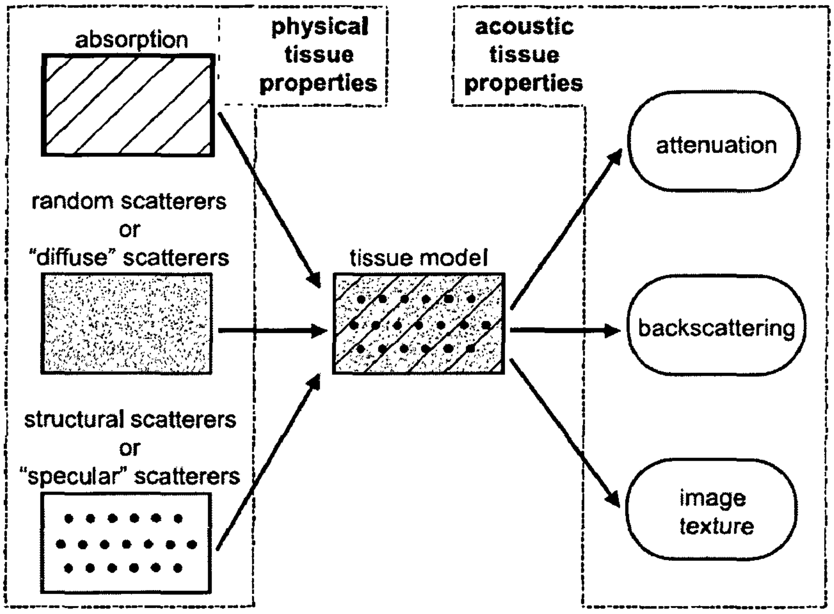

Figure 2.1: Tissue model in ultrasound imaging [13]

2.2 Speckle Model

Considerable work has been done on speckle modeling, the better model we have more accurately we can describe the features in the image. Ultrasound researchers, such as Burkhard and Wargner [14] adopted Goodman's model [15] that was derived from coherent optical imaging. The model is well suited for fully developed speckle case. For the images that contains both fully developed and partially developed speckle a general model, k distribution [16] was first introduced later in to the ultrasound imaging [17]. The clinical ultrasound B-scan images are dynamic range compressed to actually fit the display or human dynamic perceptible dynamic range. So the statistical properties of speckle are different in clinical situations. To deal with clinical B-scan images practical models are used are described below.

2.2.1 Goodman's Model

When ultrasonic waves passes through an object such as human body having internal acoustic impedance mismatches, a portion of the incident energy is reflected at the interface of the mismatches. Speckle as discussed above are a special case of scattering called diffusion scattering. Ultrasound speckle results from the coherent accumulation of random scatterings from within the resolution cell. The accumulation can be described geometrically as a random walk of component phasors.

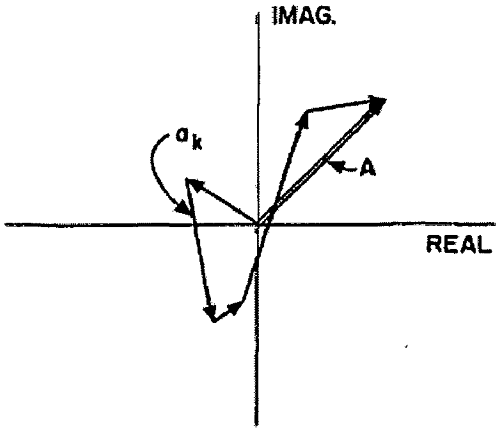

Figure 2.2: Random walk in the complex plane [15]

When the number of scatterers within one resolution element is large and the phases of the scattered waves are distributed uniformly between 0 and 2Π,the complex field amplitude has a joint probability density function (pdf) given by [14]. This phasor has real and imaginary components, a_r and a_i.

$$p(a_r, a_i) = \frac{1}{2\Pi\sigma^2} exp\left\{-\frac{a_r^2+a_i^2}{2\sigma^2}\right\}\ldots\ldots\ldots\ldots\ldots\ldots(1)$$

This is simply the product of two independent Gaussian density functions with zero mean and variance and is referred to as a circular Gaussian probability density function. For the phasor magnitude $v = [a_r^2 + a_i^2]^{\frac{1}{2}}$ the pdf

$$p(v) = \frac{v}{\sigma^2} exp\left\{-\frac{v^2}{2\sigma^2}\right\},\ v \geqslant 0\ldots\ldots\ldots\ldots\ldots\ldots\ldots(2)$$

$$= 0, \text{ otherwise}$$

and for the intensity $I = v^2$ the pdf [14],

$$p(I) = \frac{1}{2\sigma^2} exp\left\{-\frac{I}{2\sigma^2}\right\},I \geqslant 0\ldots\ldots\ldots\ldots\ldots\ldots\ldots\ldots\ldots(3)$$

$$= 0, \text{ otherwise}$$

In keeping with the common convention,we can rewrite (2) as

$$p(v) = \frac{v}{\psi} exp\left\{-\frac{v^2}{2\psi}\right\},v \geqslant 0\ldots\ldots\ldots\ldots\ldots\ldots\ldots\ldots(4)$$

$$= 0, \text{ otherwise}$$

The parameter Ψ depends on the mean-square amplitude of the particles in the scattering medium. The density function in (3) is called exponential pdf with mean equal to variance; the function in (2) and (4) is called the Rayleigh pdf. The expected value of v, $< v >$, in units of its standard deviation $\mathrm{var}^{1/2}$, is commonly called the signal-to-noise ratio (SNR) at a point SNR_0. The theoretical value of SNR for Rayleigh statistics found to be 1.91 [14]. The Rayleigh distribution is a special case of Rician distribution as shown in fig 2.3 below. Case (d) in the figure is the approximately Gaussian distribution that results from the combination of a strong distributed specular component and a weak diffuse component of the backscattere; cases (b) and (c) are similar to (d), but with weaker specularity. Finally, case (a) is the special case of pure diffuse scattering, often referred to as a "fully developed" speckle. When a coherent component is introduced to the speckle, it changes the Rayleigh pdf into a Rician pdf.

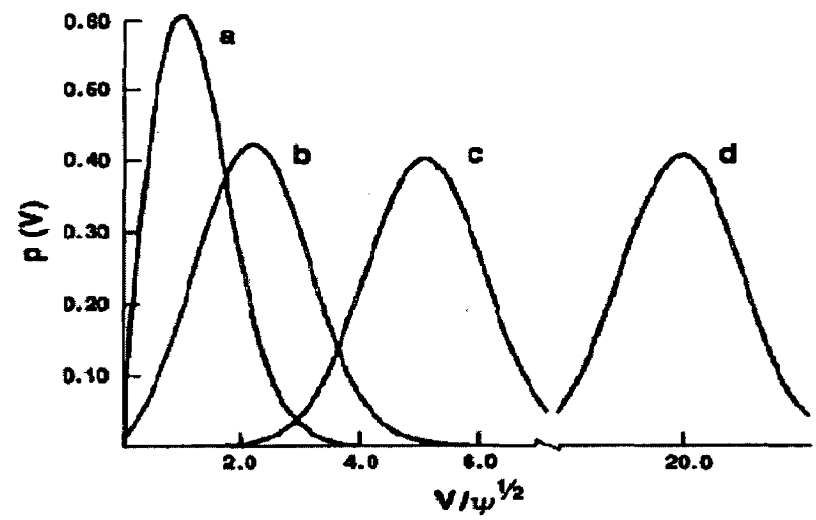

Figure 2.3: Family of Rician pdf's [14]

2.2.2 Multiplicative Speckle Noise Model

This model relates the original signal with the observed signal at each pixel value in the ultrasound image as a function of speckle noise . As discussed above the envelope detected signal has Rayleigh distribution with mean proportional to the standard deviation. This implies that speckle could be modeled as multiplicative noise. It expresses the observed intensity as a product of the original signal intensity and the speckle noise intensity. The multiplicative noise model can be written as [18]:

$$g(i,j) = u(i,j)f(i,j)\text{..........................}(5)$$

where$g(i,j)$ is the amplitude of the observed pixel and $f(i,j)$ is the noise free, $u(i,j)$is the multiplicative noise with unit mean and variance where variance $\sigma^2$and it is independent of the signal $f(i,j)$. The mean and variance are given by

$$E(u(i,j)) = E(u)\text{..............................}(6)$$

and

$$E[(u(i,j) - E(u))^2]= \sigma_u^2\text{..................}(7).$$

Images containing multiplicative noise have the characteristics that the brighter the area the noisier it is.Multiplicative noise model is the basis of various adaptive filters such as Lee, Kuan, Frost etc.

2.2.3 K-distribution Model

Goodman's model is an ideal case for speckle fully developed situation. In more general situations, when the number of scatterers is small or the effective number of scatterers is reduced the distribution of the reduced signal is more close to the lognormal. The K-distribution is given by [16] has been suggeseted to take in to account of these variations.

$$p(A) = \frac{2b}{\Gamma(N)}(\frac{bA}{2})^N k_{N-1}(bA)\text{.....................}(8)$$

where $b \geq 0$ is a scale parameters, N is the effective number of scatterers, and k_{N-1} is a Bessel function of second kind,$\Gamma(N)$ is the gamma function. For positive N, the gamma function has the simple form,

$$\Gamma(N) = N - 1!\text{.....................................}(9)$$

Fig 2.4 shows the K-distribution pdf curves at different number of effective scatterers. With N increasing the distribution moves from pre-Rayleigh(lognormal) to Rayleigh distribution. However, this distribution model does not cover the Rician case. Homodyned K-distribution and generalized K-distribution have been proposed to include the Rician distribution. Since they do not make the analytical expression simpler and this model is not considered in this work , they are not discussed in detail.

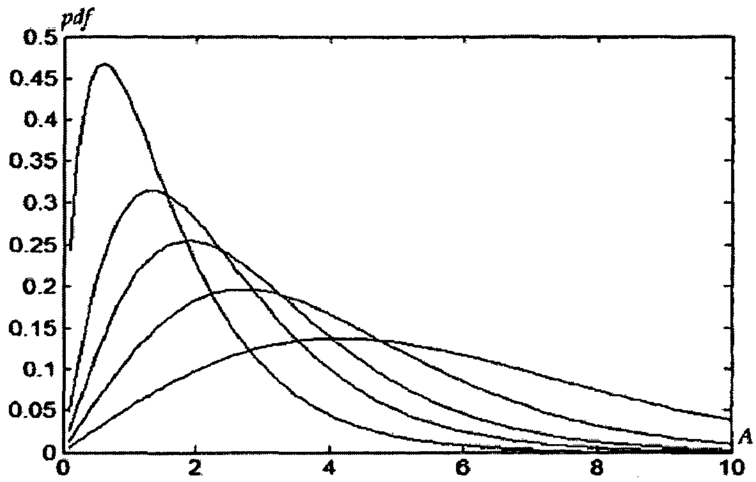

Figure 2.4: K-distribution curves with N=1,2,3,5,10 in sequential order(b=1)

2.2.4 Loupas' Model

In clinical situations B-scan images are usually dynamically range compressed. This compression changes statistics of the images and to perform image processing on such images, these changes has to be considered. To meet the dynamic range of display or the human visual perceptibility, the raw data of ultrasound image undergo dynamic range compression. The dynamic range is given by

$$DR(db) = 20log\frac{A_{max}}{A_{min}} ....(10)$$

where A is the brightness value of the data and $A_{min}$is the precision that will be preserved in the original data. Taking X as a brightness value of the compressed data,the relationship between X and A is given by

$$X_{max} - X_{min} = Dlog\frac{A_{max}}{A_{min}} ....(11)$$

where X_{min} is the minimum value of the compressed data and D is the parameter to control the degree of the compression.
D can be estimated with the following formula,

$$D = \frac{20}{DR}(X_{max} - X_{min}) ....(12)$$

For most B-scan images used, the maximum brightness value is 255 and the minimum brightness value is 0. The dynamic range compressed B-scan image is of Gaussian distribution in the region where speckle is partially developed. Speckle fully developed with coherent components follows the Rician case.

Besides, the logarithmic compression the various signal processing stages (low pass filtering, interpolation) inside the scanner modify the statistics of the original signal. The signal is no longer multiplicative in nature, as the mean is proportional to variance rather than the standard deviation [7]. If x denotes the true signal, n is a noise term which is independent of x and has mean 0 and y is the observed signal, the following signal dependent noise model (Loupas' model) can be written

$$y = x + x^{1/2}n \quad \text{.................(13)}$$

2.3 Conclusion

In this chapter various speckle models have been described based on their statistical behaviour. As seen Goodman's model is applicable only when the speckle is fully developed which is not always true. The multipliative noise model is suitable for the processing techniques which uses the envelope detected RF signal. But it cannot be used for the log-compressed image, because the log compression changes the statistics of the speckle and it is no longer multiplicative in nature. For log compressed images Loupas' model is to be used for speckle modelling. In this thesis work Loupas' model has been considered for the dynamic range compressed B-scan images.

Chapter 3

Adaptive Filtering for Speckle Reduction

3.1 Inrtoduction

In the prevoius chapter the statistics of the speckle had been described under the different conditions. Before applying any filtering technique an accurate modelling of the speckle is necessary. In this chapter the various adaptive filtering based techniques for speckle reduction have been discussed. Under the adaptive filters both adaptive weighted median (AWMF) and aggressive region grwoing (ARGF) have been implemented. These techniques make use of Loupas' model for spekcle behaviour. The adaptive filters are applied on the speckle simulated images and the real ultrasound images. For comparison of the performance: the ability to retain small details and edges i.e. sudden transitions in gray level or texture and gradual changes in gray level are taken as the yard sticks. Several quantitative measures like, figure of merit (FOM), mean square distances (MSD), contrast to noise ratio (CNR) and mean structural similarity index measure (MSSIM) have been used for this task. The details of these quantitative measures are depicted in subsequent chapter.

3.2 Adaptive Filter

In this section the adaptive filter based on the multilicative noise model and Loupas' model have been discussed. Adaptive filters take account of speckle distribution models and compute local statistics within a moving window and assign new values accordingly, leading to better result. The Lee [19], Kuan [20], and Frost filters [21], aimed at minimizing the mean square error (MSE), are derived from the speckle model, i.e., assuming speckle is a multiplicative noise random variable with mean of one. By examining the derived formulas, however, the Lee and Kuan filters can be considered as adaptive-mean filters. AWMF [7] and ARGF[9] filters are based on the Loupas' model. AWMF is an enahnced median filter and it is based on weighted median. Aggressive region growing filter (ARGF) selects a filtering region size using an appropriately estimated homogeneity value for region growth. Homogeneous regions are processed with an arithmetic mean filter. Edge pixels are filtered using a nonlinear median filter.

3.2.1 Lee Filter

The basic idea behind Lee filter is that if the variance over an area is low or constant, then the smoothing will be performed. Otherwise, if the variance is high (i.e. near edges), smoothing will not be performed. Lee filter assumes that the speckle noise is multiplicative. Thus, the filtered ultrasound image can be approximated by a linear model given as in Eq. (3.1)

$$\hat{F} = \bar{F} + k(F - \bar{F}) \qquad (3.1)$$

where $\hat{F}$ is the estimate value of the noise free pixel, $\bar{F}$ is the average value of the pixels within the filter window n_F and k_{cov} is a adaptive filter coefficient equal to

$$k_{cov} = \frac{C_z^2 - C_v^2}{C_z^2 + C_v^2} \qquad (3.2)$$

From (3.1), it is clear that in the flat parts the filtered pixel $\hat{F}$ is about to equal to the local mean $\bar{F}$. But in rapidly varying regions (containing edges), the filter output is equal to the observed pixel value F. The value of k lies between [0 1]. The COV in the alternative form of Lee filter is given as:

$$C_x^2 = \frac{C_z^2 - C_v^2}{1 + C_v^2} \qquad (3.3)$$

where $C = \frac{\sigma}{\mu}$ and C_x is COV of the noise free signal, C_z is COV for the noise affeted signal and C_v is COV for the speckle noise.

3.2.2 Adaptive Weighted Median Filter

The weighted median is a general class of median-type filters, having the weighted coefficients. The weighted median of a sequence $\{X\}$ is defined as the pure median of the extended sequence formed by taking each term X_i, w, times, where $\{w\}$, are the corresponding weight coefficients [7]. For example, if $w_1 = 2, w_2, = 3, w_3 = 2$, the weighted median of the sequence $\{X_I, X_2, X_3\}$ is given by

$$y_{wm} = median\{X_1, X_1, X_2, X_2, X_2, X_3, X_3\} \qquad (3.4)$$

By adjusting these weight coefficients smoothing characteristics of the filter can be varied. Thus it is possible to suppress noise.

As more emphasis is placed on the central weights the ability of the weighted median to suppress noise decreases but also the signal preservation increases. This is a very useful characteristic because it allows the design of filter which combines median-type properties with adjustable smoothing [7]. It can be achieved by choosing a family of weights which decrease as we move away from the center of the window. This rate of decrease is controlled by the local image content. This is the main idea behind the adaptive weighted median. In this the Loupas' model is considered for the speckle modelling.

$$y = x + x^{1/2}n \quad \text{...} (3.5)$$

Local statistics have been used to deal with the space varying image content. The mean value gives the measure of gray level while variance gives an idea about the contrast of the image. The mean and variance are defined below.
Let $X = x_{i,j}$ $i = 1, 2, 3, ..., M$ and $j = 1, 2, 3, ..., N$ be the image containing M rows and N columns with gray level $x_{i,j}$ at pixel (i, j). A region $W_{w \times w}$ of X is a connected subset of X. $W_{i,j}$ denotes a local region associated with (i, j). The two local statistical parameters: arithmetic mean and variance of image intensity are to be computed within a region as follows:

$$\mu_{i,j} = \frac{1}{w^2} \sum_{m=-\frac{w}{2}}^{\frac{w}{2}} \sum_{n=-\frac{w}{2}}^{\frac{w}{2}} (x_{i-m,j-n}) \quad \text{.......................} (3.6)$$

$$\sigma^2_{i,j} = \frac{1}{w^2} \sum_{m=-\frac{w}{2}}^{\frac{w}{2}} \sum_{n=-\frac{w}{2}}^{\frac{w}{2}} (x_{i-m,j-n} - \mu_{i,j})^2 \quad \text{................} (3.7)$$

The local variance and mean ratio of the sampled pixel in a fully developed ultrasound speckle image is used as the suitable parameter. In adaptive weighted median (AWM) the ratio $\frac{\sigma^2}{\mu}$ characterize the local image content and performs the space-varying weighted median filtering with the weight coefficients adjusted according to the local statistics of the image by using the formula,

$$w(i, j) = \left[w(K + 1, K + 1) - cd\frac{\sigma^2}{\mu} \right] \quad \text{........................} (3.8)$$

where,
c scaling constant
μ, σ^2 the local mean and variance inside the $2K + 1$ by $2K + 1$ window,
d distance of the point (i, j) from the centre of the window $(K + 1, K + 1)$,

$[x]$ denotes the nearest integer to x if x is positive, or zero if x is negative.
The selection of the weight coefficients represents a trade-off between noise reduction and signal preservation.

Results And Discussions:

Speckle Simulated Image Results : Original shape image is corrupted by Loupas' model presented in Eq.(3.5) for simulation of the speckle distortion where noise is randomly introduced by the normal probability distribution function with mean = 0 and variance = 0.2. The original and speckle-distorted image is shown in Fig.3.1(a) and Fig.3.1(b). The window size for this filter is taken as 9 x 9.

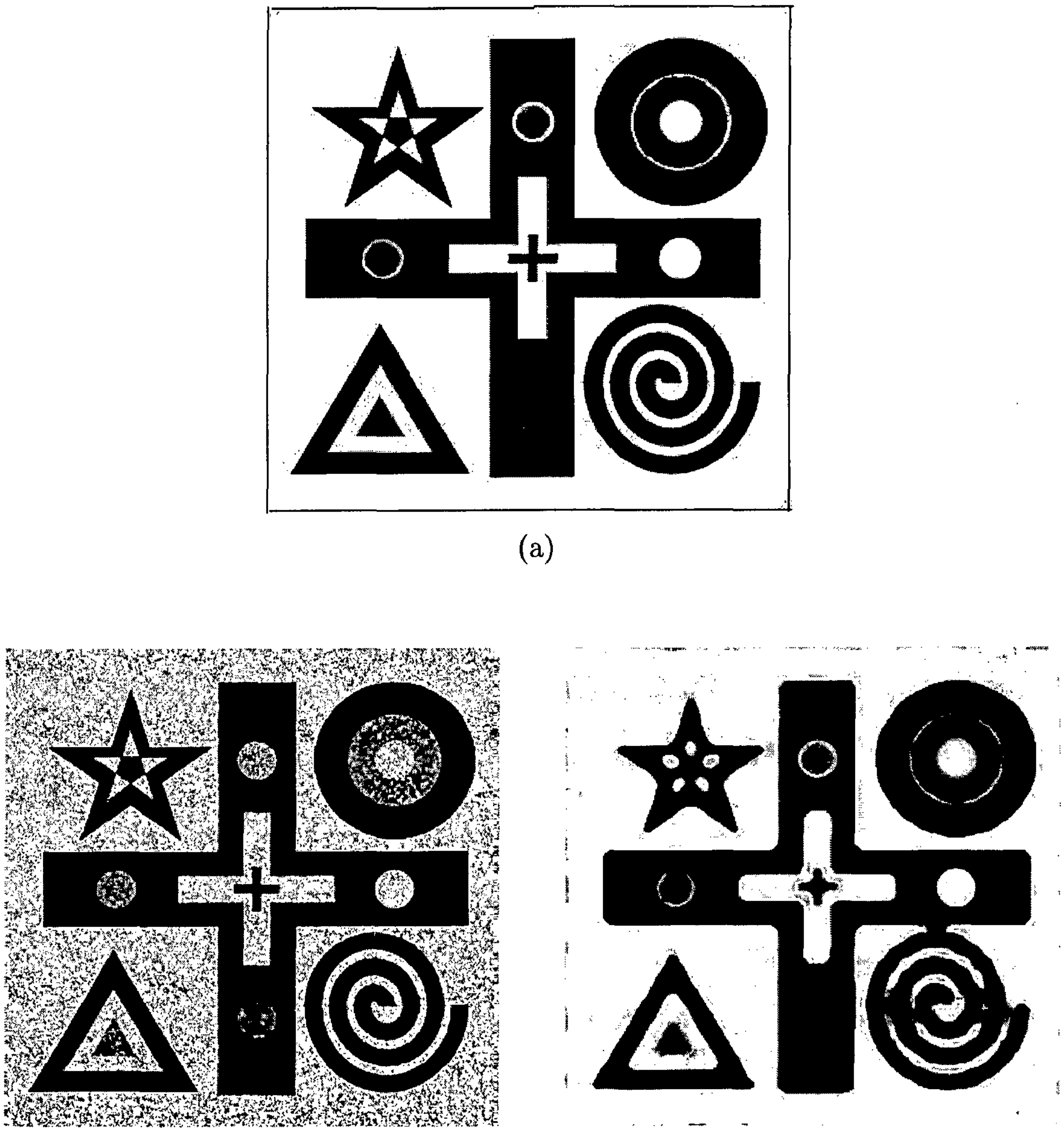

(a) (b) (c)

Figure 3.1: Shape image a) Original b) Simulated with speckle noise c) AWMF filtered

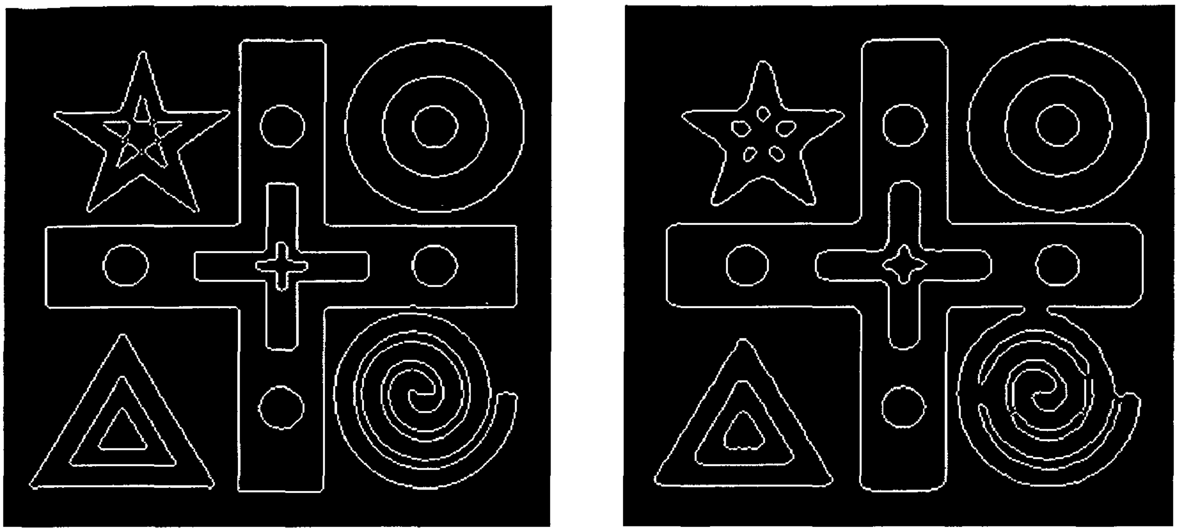

(a) (b)

Figure 3.2: Edge profile obtained using Canny opearator a) Original b) AWMF Filtered

From the fig.3.1(b) and (c) it is seen that the AWMF reduces the speckles in the image. The speckle simulated image background has bright dot like appearance which is the speckle noise. This has been smoothened by the AWMF. Also a careful look at the small circles shows that inside the circles smoothing has occured thereby reducing the speckle noise. But it has also caused blurring in the output image. The spiral shape in the image have been blurred and the rounding of corners have taken place in the centrally placed rectangular structure. To see the edge preservation ability of the AWMF an edge profile is obtained by applying the Canny operator on the original and the filtered image. As shown in the fig 3.2 , the edge profile of the original image and the filtered image, the smearing of the edges occurs as a result of filtering. The spiral structure has lost its sharp edges and has smeared with the upper rectangular strip whereas in the original image their boundaries are distinctively visible.

Real Ultrasound : The AWMF is applied on the real B-scan image of the portal vein. This image has the diagnostic features and the cavities. The fine details have been marked in the image. Fig 3.3 shows the result of filtering the ultrasound B-scan image. As seen in the figure 3.3 (b) the AWMF has smoothened the image background, thus reducing the speckles. But the fine details marked with arrows (shown in fig 3.3 (a)) have been lost. If the region around the cavities is to be studied then AWMF can be useful.

From the above results it can be concluded that AWMF causes smoothing of the images at the cost of losing the fine details. If speckle reduction is only the main consideration then AWMF can be used.

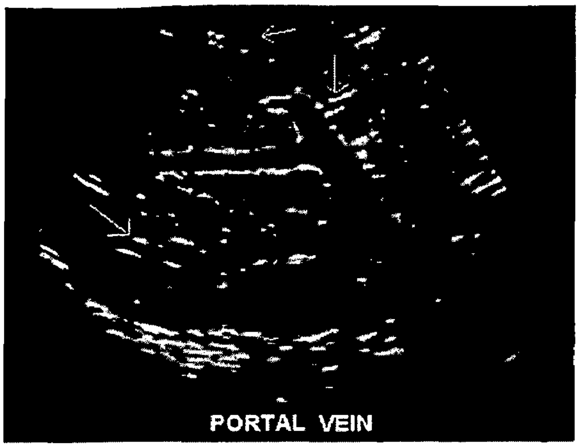

(a)

(b)

Figure 3.3: Portal vein image a) Original b) AWMF filtered

3.2.3 Aggressive Region Growing Filter (ARGF)

Several region-based adaptive filter techniques have been developed for speckle reduction but there are no specific criteria to choose the size for region growing in the post processing of the filter. The size of a region appropriate for one local region may not be appropriate for the other region. Generally, a large region size is used to smooth speckle and a small region to preserve the edges in an image. Selection of the correct size of a region involves a tradeoff between speckle reduction and edge preservation. To overcome this type of problem, the filter described in this section is basically based on the aggressive region growing approach where region growth and region smoothing are processed by the first order statistics.The ARGF [9] procedure constructs a homogeneous filtering region whose size is adjusted by shrinking and growing to make it of maximal size within the pre-specified upper limit. This algorithm has three stages: selection of a seed region, contraction of this seed region until it is homogeneous and expansion of this homogeneous region till it satisfies the homogeneity criterion or its size exceeds a pre-specified limit. The block diagram of the ARGF method is shown below in fig 3.4. The details of the approach are presented below.

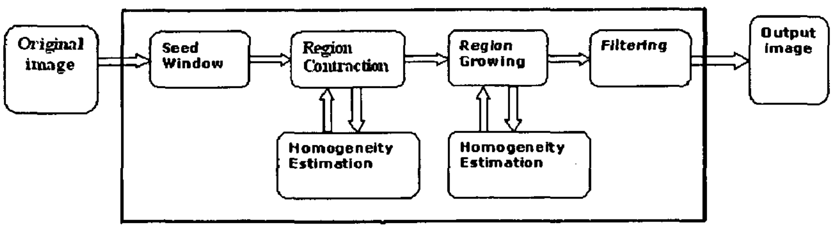

Figure 3.4: Diagram of ARGF method[9]

Homogeneity model using first order statistics :

In uniformly spatially distributed speckle regions, the amplitude of fully developed speckle has been determined to follow a Rayleigh distribution with the mean proportional to the standard deviation. The logarithmic compression of the echo amplitude data used in ultrasound scanner may change the statistics of the speckle features.As an example, Fig. 3.5 and 3.6 show the gray-level histograms for uniform speckle regions in a real ultrasound image. It is observed that the distribution of speckle is Gaussian-shaped rather than Rayleigh-shaped. It means the mean is directly proportional to the variance rather than standard deviation. For the signal dependent noise model using the linear relationship between mean and standard deviation proposed by Loupas et al. [7] expressed as follows:

$$y = x + x^{1/2}n \text{..................}(3.9)$$

The local variance and mean ratio of the sampled pixelcan be used to describe the homogenity of a particular region..From Eq. (3.6) and (3.7) the parameter representing the ratio of local variance to mean of the pixel (i, j) in Eq. (3.5) is calculated as follows:

$$h(i,j) = \frac{\sigma_{i,j}^2}{\mu_{i,j}} \text{......................}(3.10)$$

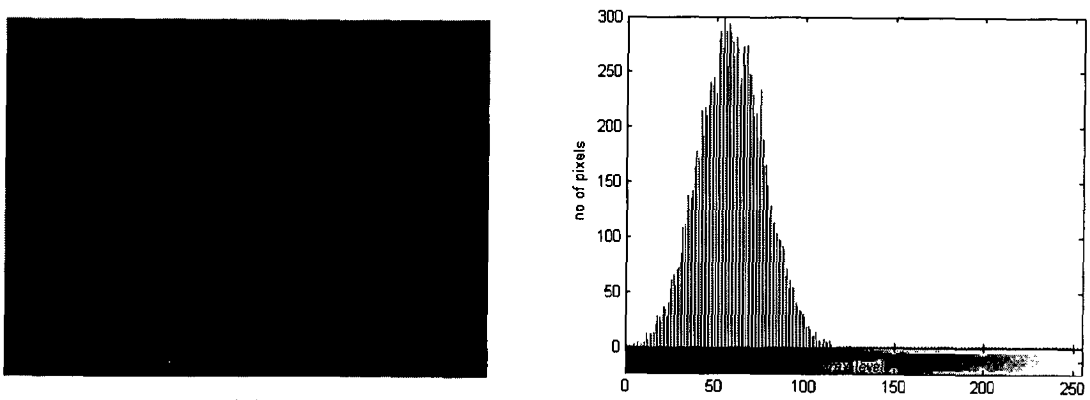

(a) (b)

Figure 3.5: Uniform speckle ultrasound image: (a) Original image and (b) Gray level histogram.

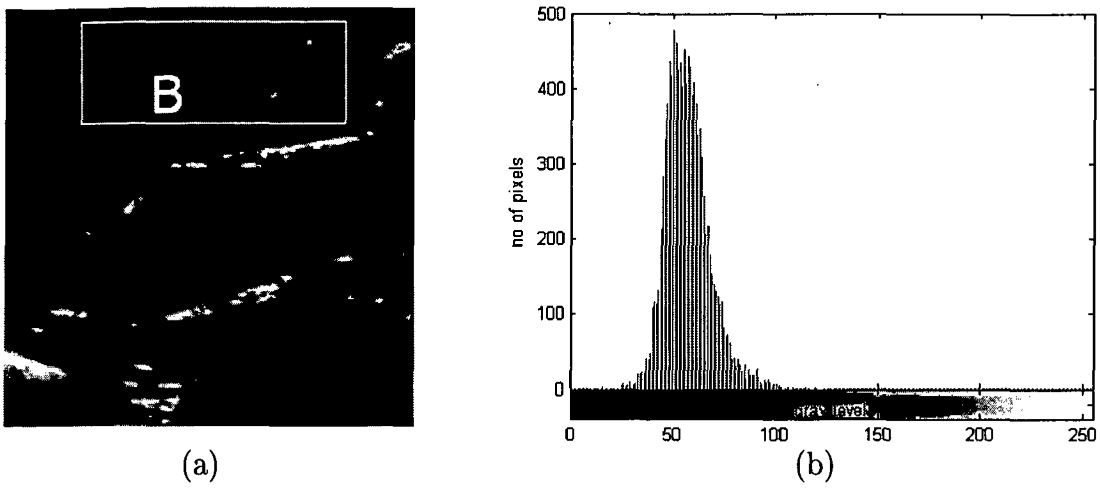

Figure 3.6: a) Original ultrasound image, (b) Gray level histogram of region B

In the adaptive filtering operation, $h(i,j)$ is a homogeneity factor, which is used to determine whether the local region is homogeneous, or not. Normally homogeneous regions have small value of $h(i,j)$ whereas the regions containing edges have high values. The parameter h_0 is a homogeneity threshold to decide the regions whether they are homogeneous or not by comparing the homogeneity factor with it. If is smaller than h_0 then regions are considered to be homogeneous and are smoothened out. In other case, these regions contain edges and are preserved.

Homogeneity criteria

The homogeneity parameter depends on the region size so an adjustable homogeneity criteria is selected based on local first order statistics. Homogeneity is measured at different locations in uniform speckle regions using different region sizes. Fig.3.7 plotted homogeneity versus region size for the B-scan of portal vein image, where it suggests a parameterized model for h_0 followed by Eq. (3.11):

$$h_0 = \frac{a||w||+u}{b+||w||} \qquad (3.11)$$

where $||w||$ is window size of M x M . Here a, b and u are evaluated by nonlinear least square regression parametric fitting. Eq. (3.11) is basically homogeneity model used for the adaptive homogeneity criterion. In this criterion, h_0 describes statistical specifications of homogeneous regions and is adaptively determined on the basis of current size of region in the image.

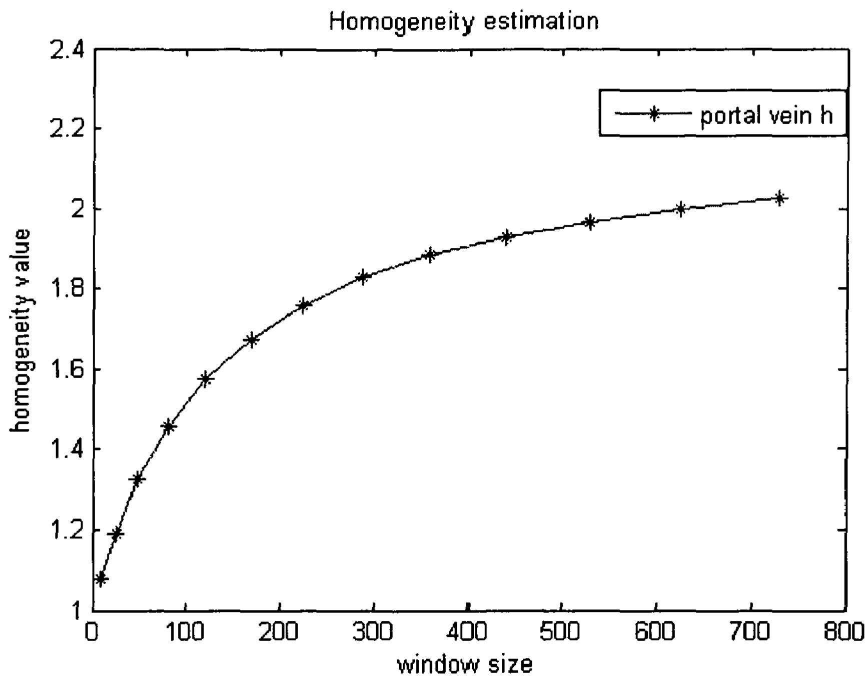

Figure 3.7: Homogeneity vs window size for portal vein image

While homogeneity h increases as the region size grows larger, its standard deviation decreases.Therefore, the following parameterized model for the standard deviation σ_0 is proposed:

$$\sigma_o = c + kexp(-d \parallel w \parallel)\text{..........................}(3.12)$$

where c and k are parameters with values that are estimated empirically. The model parameters are obtained via nonlinear regression based on observed homogeneity measurements.

The algorithm is defined below:

Algorithm (ARGF)

For each pixel (i, j)

1. Define an initial seed region Wij to be of size 11 x 11 and centered at (i, j).
2. Region contraction
   (a) Calculate the homogeneity factor $h(i, j)$ of Wij.
   (b) Calculate the homogeneity threshold h_0 and σ_0 corresponding for the window size $\parallel W \parallel$ to the current Wij and depth d in the image.
   (c) While $(h(i, j) > h_0 + \sigma_0)$ and $\parallel W \parallel > S_{min}$, shrink the region and go to Step 2.a. Here S_{min} is the lower size limit. If $(h(i, j) \leq h_0 + \sigma_0)$ is not true before $\parallel W \parallel \leq S_{min}$ then go to Step 4.b.

3. Region growing

   (a) Calculate the homogeneity factor $h(i, j)$ of the current region.

   (b) Update the homogeneity criterion h_0 and σ_0 corresponding for the window size $\| W \|$to the current Wij and depth d in the image.

   (c) While $(h(i, j) \leq h_0 + \sigma_0)$, $h(i, j)$ changes by less than σ_0 and $\| W \| < S_{max}$, expand the region and go to Step 3.a. Here S_{max} is the upper size limit.

4. Filtering

   (a) If $\| W \| > w_0$, the value of the output pixel at (i, j) is the trimmed arithmetic mean of the pixels in Wij.

   (b) If $\| W \| \leq w_0$, the value of the output pixel at (i, j) is the median of the pixels in Wij.

Seed window size:
The initial seed region Wij is 11 x 11 pixels in size and centered at (i, j). In this, a size of 7 x 7 is considered minimal (hence, $S_{min} = 49$), since speckle artifacts can sometimes exceed this size, causing an incorrect classification of a seed region inside a speckle artifact as homogeneous.

Region Contraction :

The initial seed region Wij is contracted by removing its outermost rows and columns and contraction is repeated until the homogeneity $h(i, j)$ agrees with the estimate h_0 predicted by Eq.(3.11) to within a tolerance σ_0 predicted by Eq.(3.12). If the contraction procedure fails to find a homogeneous region before the size shrinks to the minimal threshold value S_{min}, a pixel is assumed to be an edge, a 3 x 3 median filter is applied to preserve edge details, and processing continues at Step 1 with the next pixel.

Region Growing :

After the contraction procedure the next step is to find a maximum homogenous region around the entral pixel by region growing. A systematic region growing method expands the region one side at a time is used. The direction of expansion cycles clockwise i.e. north, south, east, west. As in the region contraction procedure, the estimated and predicted homogeneities are compared after each expansion to determine whether region expansion should continue.

Filtering :

In the ARGF method, the trimmed mean filter is applied in the homogeneous region after the region growing procedure. Pixels in a non-homogeneous region are assumed to contain resolvable edges and are processed by a small median filter (3 x 3) to preserve edge details. A trimmed mean filter is used to preserve the image contrast. It can be defined as,
Let W_{ij} be the current filtering region and $(\hat{\mu_{w_{ij}}}, \hat{\sigma_{w_{ij}}})$ be the sample mean and standard deviation of W_{ij}. The original region W_{ij} is trimmed to construct the new pixel set P_{ij} :

$$P_{ij} = \{x_{kl} \mid (k,l) \in W_{ij} \cap \mid x_{kl} - \hat{\mu_{w_{ij}}} \mid < \hat{\sigma_{w_{ij}}}\} \text{ ....(3.13)}$$

The output pixel value at (i, j) is the mean value of the set P_{ij};

$$y_{ij} = \frac{1}{\|P_{ij}\|} \sum_{x_{kl} \in P} x_{kl} \text{ ....(3.14)}$$

Results And Discussions

Speckle Simulated Image Results: Original shape image is corrupted by Loupas' model presented in Eq.(3.5) for simulation of the speckle distortion where noise is randomly introduced by the normal probability distribution function with mean = 0 and variance = 0.2. The original and speckle-distorted image is shown in Fig.3.8(a) and Fig.3.8(b). The window size for this filter is taken as 13 x 13 and the values of the parameters were found by making the homogeniety model for the shape image.

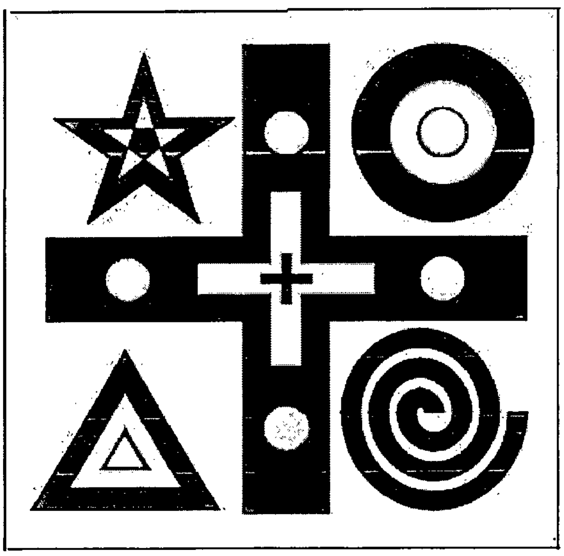

(a)

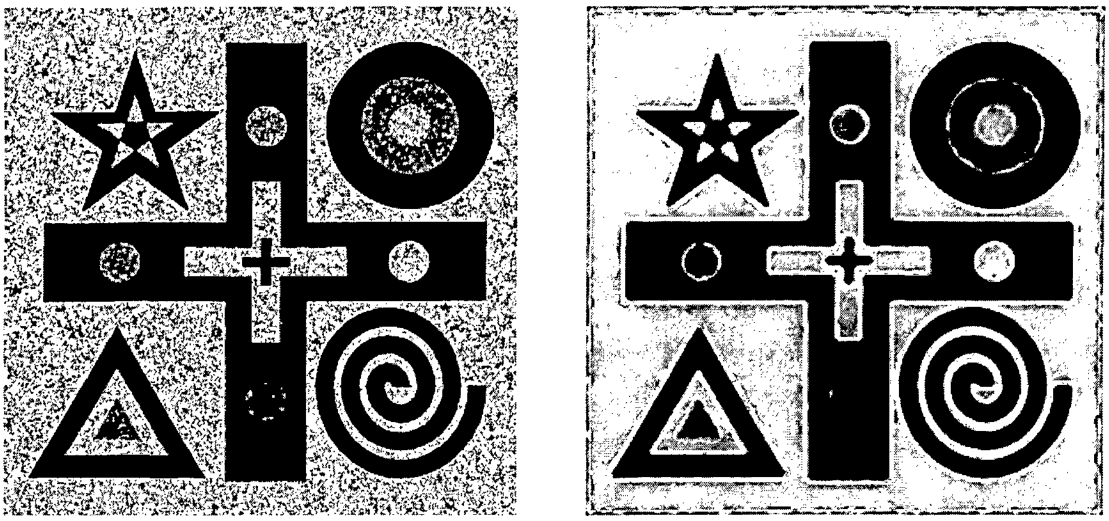

(b) (c)

Figure 3.8: Shape image a) Original b) Simulated with speckle noise c) ARGF filtered

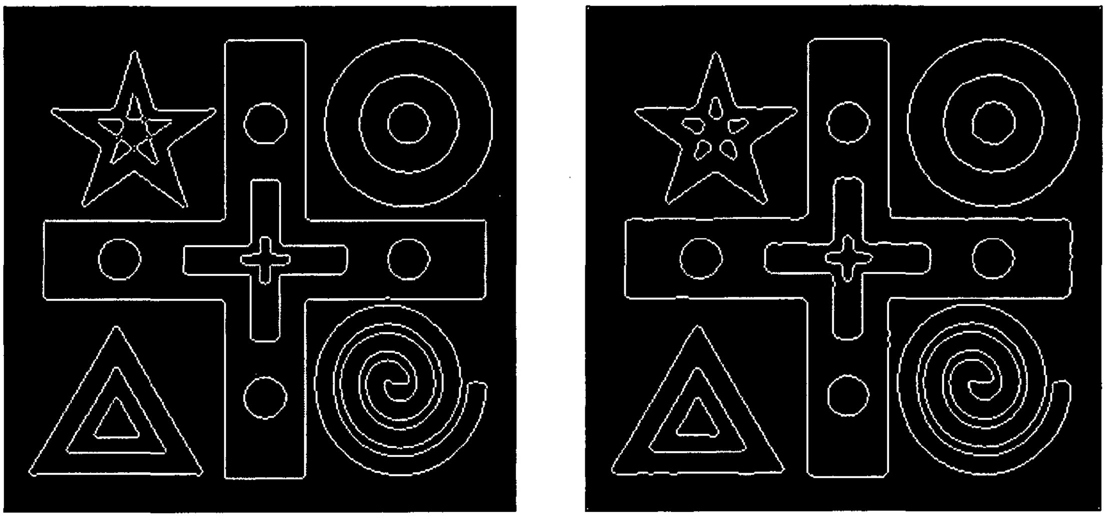

(a) (b)

Figure 3.9: Edge profile a) Original b) ARGF Filtered

From the fig.3.8 (b) and (c) it can be seen that the ARGF has reduced the speckles in the image. The speckle simulated image background has bright dot like appearance which is the speckle noise. This has been smoothened by the ARGF but the background contrast has changed slightly, this could be due to region growing and region contraction procedure. The granular appearance inside the the small circles due to speckle noise has been reduced. But it has also caused more smoothening in the output image. To test the edge preservation ability of the ARGF an edge profile is obtained by applying the Canny operator on the original and the fitered image. As shown in the fig 3.9 , the edge profile of the original image and the filtered image, the star shape as shown in fig 3.9 (a) has lost its sharp edges, otherwise other edges

By varying the parameters found, we can control the smoothing level in the images, as shown in fig3.11(a) Mode 1 and (b) Mode 2. If further segmentation is required, then ARGF can provide good results because the speckles have been removed and their texture will not interefere with the segmentation proceess.

3.3 Conclusion

The adaptive filters AWMF and ARGF are applied on the speckle simulated images and the ultrasound B-scan image. From the results it is seen that ARGF is better at reducing the speckles and retaining the features. AWMF reduces the speckles effectively , but very fine details are lost. ARGF can be used as a preprocessing step when auto segmentation is to be done. In ARGF region expansion step takes more computation time.

Chapter 4

Anisotropic Diffusion for Speckle Reduction

4.1 Introduction

This chapter describes the anisotropic diffusion technique for the speckle reduction in B-scan images. In the previous chapter adaptive filters were implemented and it was observed that these filters are very sensitive to the size and shape of the kernel window. Given a filter kernel window that is too large (compared to the scale of interest), over-smoothing will occur and edges will be blurred. A small kernel size will decrease the smoothing capability of the filter and will leave speckle. In term of the window shape, a square window will lead to corner rounding of rectangular features that are not oriented at perfect 90^0 rotations. Also the existing filters do not enhance edges-they inhibit smoothing near edges. When any portion of the filter window contains an edge, the coefficient of variation will be high and smoothing will be inhibited. Therefore, noise/speckle in the neighborhood of an edge (or in the neighborhood of a point feature with high contrast) will remain ever after filtering.

In this chapter partial differential equation based approaches have been discussed which are used for image denoising with edge preservation. These methods are either based on the axiomatic approach of non linear scale space or on the variational approach of energy function minimization. The PDE based speckle reduction approach allows the generation of an image scale space (a set of filtered image that vary from fine to coarse level) without bias due to filter window size and shape. The PDE based approaches not only preserves the edges but also enhance it by inhibiting diffusion across the edges but allowing diffusion on either side of the image. This approach is adaptive and does not use hard threshold to alter performance in homogenous region or in regions near the edges and small features [10, 11]. A partial differential equation (PDE) approach to speckle removal called speckle reducing anisotropic diffusion (SRAD) has been developed [10]. The SRAD algorithm is applied on both the synthesized (simulated) and the real ultrasound images.

4.2 Diffusion Techniques

4.2.1 Linear Diffusion:

It is the simplest PDE method for smoothing images. Diffusion can be defined as a process that equilibrates concentration gradient without creating or destroying mass[23]. This physical observation can be easily cast in a mathematical formulation. The equilibrium property is expressed by *Fick's law*

$$j = -D.\nabla u \text{..................................} (4.1)$$

This equation states that a concentration gradient ∇u causes a flux j which aims to compensate for this gradient. The relation between ∇u and j is described by the diffusion tensor D, a positive definite symmetric matrix. The case where j and ∇u are parallel is called isotropic. Then we may replace the diffusion tensor by a positive scalar-valued diffusivity g. In the general anisotropic case, j and ∇u are not parallel. The observation that diffusion does only transport mass without mass destroying it or creating new mass is expressed by the continuity equation.

$$\partial_t u = -divj \text{..................................} (4.2)$$

where t denotes the time.
Putting eq (4.1) in to the continuity equation we get the diffusion equation :

$$\partial_t u = -div\,(D.\nabla u) \text{........................} (4.3)$$

This equation appears in many many physical transport process. In the context of heat transfer it is called heat diffusion equation. The solution presented in Eq. (4.3) of this heat equation at a particular time t is the convolution of the original image with 2D Gaussian kernel G_σ of variance $\sigma = \sqrt{2t}$:

$$u_{(t)} = u_n \star G_\sigma \text{..........................} (4.4)$$

where $G_\sigma = \frac{1}{2\Pi\sigma^2} exp(-\frac{x^2+y^2}{2\sigma^2})$ and $\sigma = \sqrt{2t}$

In image processing it is interpreted as concentration of gray value at a point. The diffusion tensor does not have to be a constant : it is often chosen as the function of the local image structure. This leads to a class of nonlinear diffusion filters. Three cases are relevant for image processing:

1. linear isotropic diffusion filters using a constant diffusivity.

2. nonlinear isotropic diffusion filters with diffusivities being adapted to the local image structure.

3. nonlinear anisotropic diffusion filters with diffusion tensors being adapted to the local image structure.

4.2.2 Nonlinear Diffusion

Perona - Malik formulation

In the standard linear scale-space approach, the true location of a boundary is not directly available in the coarse scale image. The locations of the edges at the coarse scales are shifted from their actual locations. There is additional problem with the images using linear scale space filtering i.e., it destroys the edge junctions, which contain important spatial information for boundary detection.

Considering above as motivation, Perona and Malik [12], in their pioneer work have suggested following nonlinear scale space criteria for generating multi-scale description of image:

1. Casuality: Any feature at a coarse level of resolution is required to possess a (not necessarily unique) "cause" at a finer level of resolution although the reverse need not be true. In other words, no spurious detail should be generated when the resolution is diminished.

2. Immediate Localization: At each resolution, the region boundaries should be sharp and coincide with the semantically meaningful boundaries at that resolution.

3. Piecewise Smoothing: At all scales, intraregion smoothing should occur preferentially over interregion smoothing.

To satisfy these criteria, Perona-Malik proposed to adapt the diffusion to the local image characteristics by introducing a space- and time-variant diffusion coefficient $c(x, y, t)$, and formulated the following nonlinear diffusion equation. They formulated the ansotropic diffusion filter as a diffusion process that encourages intraregion smoothing while inhibiting interregion smoothing. The anisotropic diffusion equation is given by:

$$\frac{\partial F}{\partial t} = div(c(x, y, t)\nabla F) \qquad (4.5)$$

where c is the conduction coefficient lying between [0,1]. If c is a constant it reduces to isotropic heat diffusion equation. In this case, all locations in the image including edge are smoothened equally. If we want to encourage smoothing within a region in preference to smoothing across the boundaries, this could be achieved by setting the conduction coefficient to be 1 in the interior of each region and 0 at the boundaries. The blurring would then take place separately in each region with no interaction between regions. The region boundaries would remain sharp. $c(x, y, t)$ is a monotonically dcreasing function of the image gradient:

$$c(x, y, t) = f(\nabla F) \text{.................................} (4.6)$$

Although many monotonically decreaing continous functions of ∇F would suffice as diffusion function , the two functions have been suggested by Perona-Malik:

$$c_1\|\nabla F\| = exp(-\frac{\|\nabla F\|^2}{K^2}), \text{ and } c_2\|\nabla F\| = \frac{1}{1+(\|\nabla F\|/K)^2} \text{ ....} (4.7)$$

where K is a fixed gradient threshold that differentiate between the low and high contrast area. It is called as diffusion constant or flow constant. The behaviour of the filter depends on the value of K. These functions are plotted in fig4.1(a) & (b).

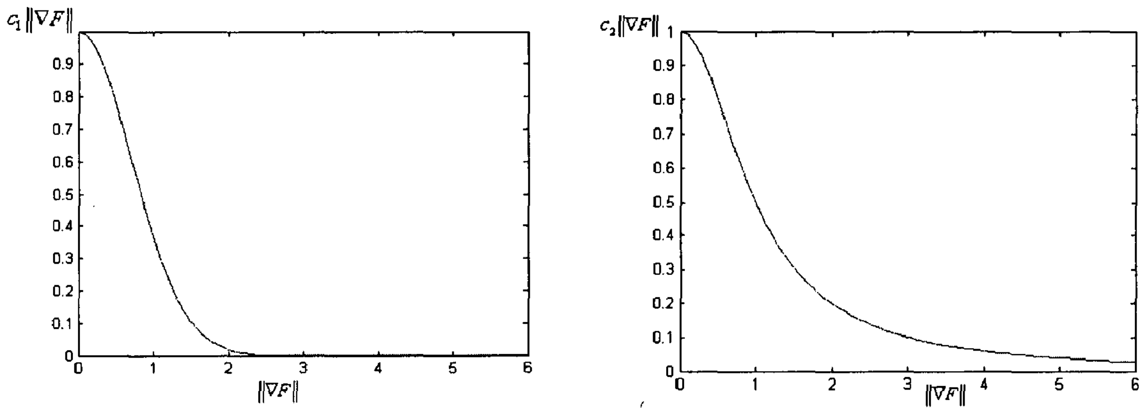

(a) (b)

Figure 4.1: Perona-Malik diffusivity (a) $c_1\|\nabla F\|$ and (b) $c_2\|\nabla F\|$

To clarify the effect of K , and the diffusion function, on the diffusion process, we define a flow function:

$$\Phi(\nabla F) = c(\|\nabla F\|).\|\nabla F\| \text{..............................} (4.8)$$

The flow functions Φ_1 and Φ_2 corresponds to diffusion functions c_1 and c_2. The flow increases with the gradient strength to the point where$|\nabla F| = K$, then decreases to zero. This behavior implies that the diffusion process maintains homogeneous regions (where $|\nabla F| \ll K$) since little flow is generated. Similarly, edges are preserved because the flow is small in regions where$|\nabla F| \gg K$. The greatest flow is produced when the image gradient magnitude is close to the value of K. Therefore, by choosing K to correspond to gradient magnitudes produced by noise, the diffusion process can be used to reduce noise in images. Assuming an image contains no discontinuities, object edges can be enhanced by choosing a value of K slightly less than the gradient magnitude of the edges. These features of nonlinear anisotropic diffusion are shown in fig 4.2

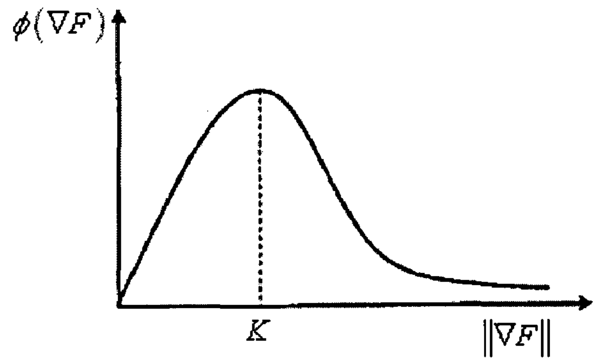

Figure 4.2: Flow function plotted as a function of image gradient

Discrete Implementation

In practical problems the image is sampled at the nodes(pixels) of a fixed equidistant grid. Thus the diffusion filter has to be discretized. For the discretization, the following three key ideas help to map the problem from the continuous domain to the discrete domain [12].

1. In the discrete domain, a gradient or derivative can be approximated as the difference in intensity between neighboring elements in the image.

2. The flow function introduced in $\Phi(\nabla F) = c(\|\nabla F\|).\|\nabla F\|$ can be calculated independently for each of the neighboring elements.

3. The filter is iterative; the right hand side of Eq. (3.4) describes the change in image intensity produced by single iteration of the filter.

Eq. (3.4) can be discretized on a square lattice with brightness value associated to the vertices and flux functions to the arcs (Fig. 4.3). 4-nearest neighbor discretization of the Laplacian operator has been used as:

$$F_{i,j}^{t+1} = F_{i,j}^{t} + \Delta t\,[c_N.\nabla_N F + c_S.\nabla_S F + c_E.\nabla_E F + c_W \nabla W F]_{i,j}^{t} .....(4.9)$$

where $0 \leq \triangle t \leq \frac{1}{4}$ for the numerical scheme to be stable. The nearest neighbor differences are :

$$\nabla_N F_{i,j} = F_{i-1,j} - F_{i,j}$$
$$\nabla_S F_{i,j} = F_{i+1,j} - F_{i,j}$$
$$\nabla_{\mathcal{E}} F_{i,j} = F_{i,j+1} - F_{i,j}$$
$$\nabla_{\mathcal{W}} F_{i,j} = F_{i,j-1} - F_{i,j}$$

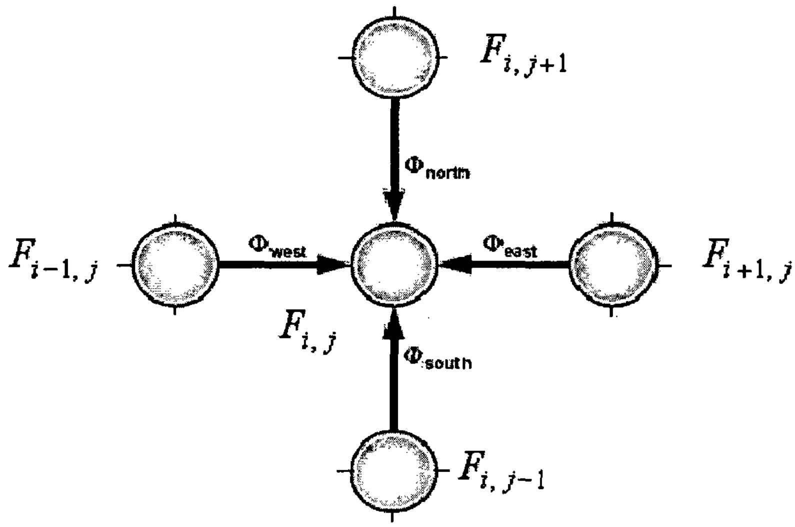

Figure 4.3: Discretization for 2D diffusion among the pixels

Diffusion coefficients are updated in each step as functions of the brightness gradient. The value of gradient can be computed on different neighborhood structures achieving different compromises between accuracy and locality.

$$c^t_{Ni,j} = c\left(\|(\nabla_N F)^t_{i,j}\|\right)$$
$$c^t_{Si,j} = c\left(\|(\nabla_S F)^t_{i,j}\|\right)$$
$$c^t_{Ei,j} = c\left(\|(\nabla_E F)^t_{i,j}\|\right)$$
$$c^t_{Wi,j} = c\left(\|(\nabla_W F)^t_{i,j}\|\right)$$

Eq (4.5) can be written as:

$$F^{t+1}_{i,j} = F^t_{i,j} + \triangle t(\Phi_N + \Phi_S + \Phi_E + \Phi_W)^t_{i,j} \quad \text{(4.10)}$$

where $\Phi(\nabla F) = c(\|\nabla F\|).\|\nabla F\|$

4.3 Speckle Reduction Anisotropic Diffusion Filter

SRAD is the edge sensitive diffusion for speckled images corrupted with signal-dependent, spatially correlated multiplicative noise. It utilizes the instantaneous coefficient of variation as in the adaptive filtering, which is a function of the local gradient magnitude and Laplacian operators. In the presence of the speckle noise, speckle reducing anisotropic diffusion gives better results over the traditional speckle removal filters and the conventional anisotropic diffusion filters. SRAD is based on the same minimum mean square error (MMSE) approach to filtering as Lee and Kuan filters.

From [10] the relationship of lee filter discussed in chapter3, with conventional anisotropic diffusion shows that:

$$\hat{I_{i,j}} = I_{i,j} + \frac{1}{\eta_s} div\left[(1 - k_{i,j})\nabla I_{i,j}\right] \quad (4.11)$$

The relationship shown in Eq. (4.11) is similar to the discrete form of the anisotropic diffusion where $c(\|\nabla I_{i,j}\|) = (1 - k_{i,j})$, η_s represents the spatial neighborhood of pixel at (i, j) and $|\eta_s|$ is the number of pixels in the window (usually four, except at the image boundaries).
The Lee filter and enhanced Lee filter process a current pixel based on its intensity and the intensities of neighboring pixels inside a fixed square window. Thus, these two filters have no mechanism to enhance edges or feature structures within a window. The modification of the Lee filter to include directional sensitivity and filtering perpendicular to the edge direction would significantly enhance the ability to remove the speckle in the vicinity of edges and small features.

Coefficient Of Variation:

Similar to the coefficient of variation in the Lee filter, a discritized version of the coefficient of variation applicable to PDE has been developed[10].

$$C_{i,j}^2 = \frac{\left[I_{i,j}^2 + \frac{1}{|\eta s|}\nabla^2 I_{i,j}^2\right]}{\left[I_{i,j} + \frac{1}{|\eta s|}\nabla^2 I_{i,j}\right]^2} - 1 \quad (4.12)$$

As $C_{i,j}$ is usually called local coefficient of variation, we call the function q the instantaneous coefficient of variation. It combines a normalized gradient magnitude operator and a normalized Laplacian operator to act like an edge detector for speckled imagery. High relative gradient magnitude and low relative Laplacian tend to indicate an edge. Instantaneous coefficient of variation (ICOV), $q(t)$ is:

$$q(i, j : t)^2 = \frac{\frac{1}{2}(\frac{|\nabla I|}{I})^2 - \frac{1}{16}(\frac{\nabla^2 I}{I})^2}{\left[1 + \frac{1}{4}(\frac{\nabla^2 I}{I})\right]^2} \quad (4.13)$$

The diffusion coefficient for anisotropic diffusion using ICOV becomes:

$$c_1(q) = exp\{-[q^2(i,j;t) - q_0^2(t)] / [q_0^2(t)(1+q_0^2(t))]\} \quad (4.14)$$

$$c_2(q) = \frac{1}{1+[q^2(i,j;t)-q_0^2(t)]/[q_0^2(t)(1+q_0^2(t))]} \quad (4.15)$$

$q_0(t)$ is the speckle scale function obtained by median absolute deviations (MAD)[27]. MAD is defined as follows :

$$MAD(\nabla I) = median\{||\nabla F - median(||\nabla F||)||\} \quad (4.16)$$

$$q_0(t) = \frac{c' MAD(\nabla F)}{\sqrt{2}} \quad (4.17)$$

where $c' = 1.4826$ is derived from the fact that the MAD of a zero-mean Gaussian distribution with unit variance is $1/1.4826$.
The instantaneous coefficient of variation $q(i,j;t)$ serves as the edge detector in speckled imagery. The function exhibits high values at edges or on high-contrast features and produces low values in homogeneous regions. Similar to the parameter k in (4.4), the speckle scale function $q_0(t)$ effectively controls the amount of smoothing applied to the image by SRAD.
Finally, by approximating time derivative with forward differencing, the numerical approximation to the differential equation is given by :

$$I_{i,j}^{n+1} = I_{i,j}^{n} + \frac{\triangle t}{4} d_{i,j}^{n} \quad (4.18)$$

where $d_{i,j}^n$ is the divergence of $c(.)\nabla I$ as in anisotropic diffusion equation.

4.3.1 Results and Discussions:

SRAD algorithm is applied on speckle simulated image (shown in fig 4.4) and the real ultrasound image. In implementing the speckle reduction anisotropic diffusion algorithm, a fixed number of iterations and time step= 0.05 is used.
The output of SRAD shown in fig 4.4 is obtained for 260 iterations and $\triangle t = .05$. From the fig 4.4 (b) & (c) it is clear that SRAD has been able to reduce the speckle noise. The bright dots in the form of speckle noise have been completely smoothed giving a smooth background. Also the fine details are retained. If we look at the shapes of different patterns (circle, rectangle, star) in the filtered image, it is observed that their boundaries are delineated and well defined.

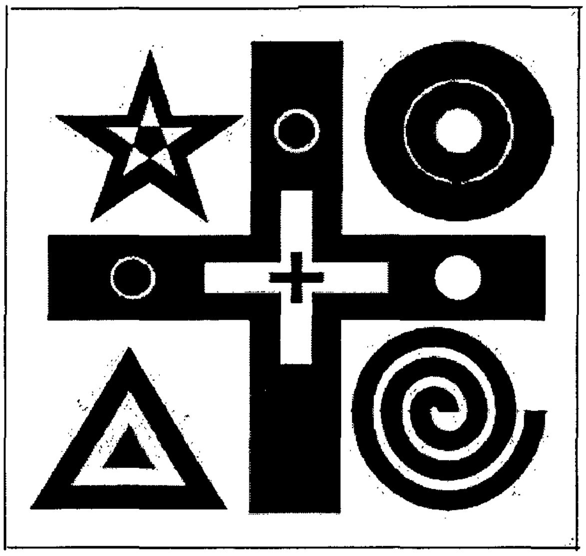

(a)

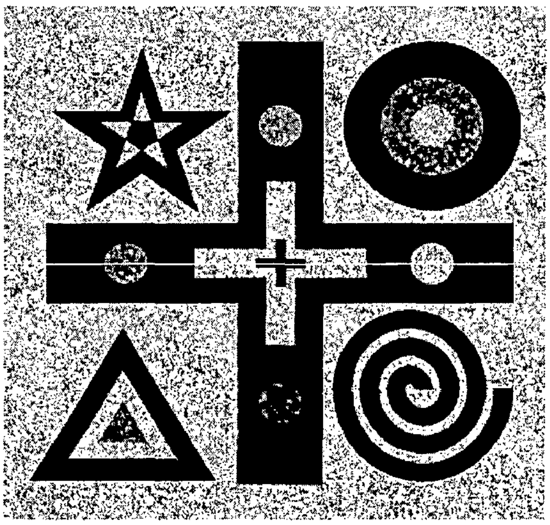

(b)

(c)

Figure 4.4: Shape image a) Original b) Simulated with speckle noise c) SRAD filtered

To test the edge preservation ability of SRAD, the edge profile of the filtered image and the original image is obatined using the Canny operator. As shown in fig 4.5 (a) and (b), the SARD technique has preserved the fine and sharp edges of the patterns in the shape image. For the synthetic image, number of iterations is 20, 60, 100, 140, 180, 220, 260 and 300 and the time step $\triangle t$ is 0.05. As the number of iterations increases the smoothing increases. This behaviour of SRAD is depicted in fig 4.6. Image obtained after 20,100,220 iterations still has speckle noise. The final filetered image is shown below in fig 4.6 (d). To see the gray level variation with the number of iteration a gray level profile along the line marked in the speckled image(fig 4.4 (a)) has been shown in fig 4.7 after a certain number of iterations.

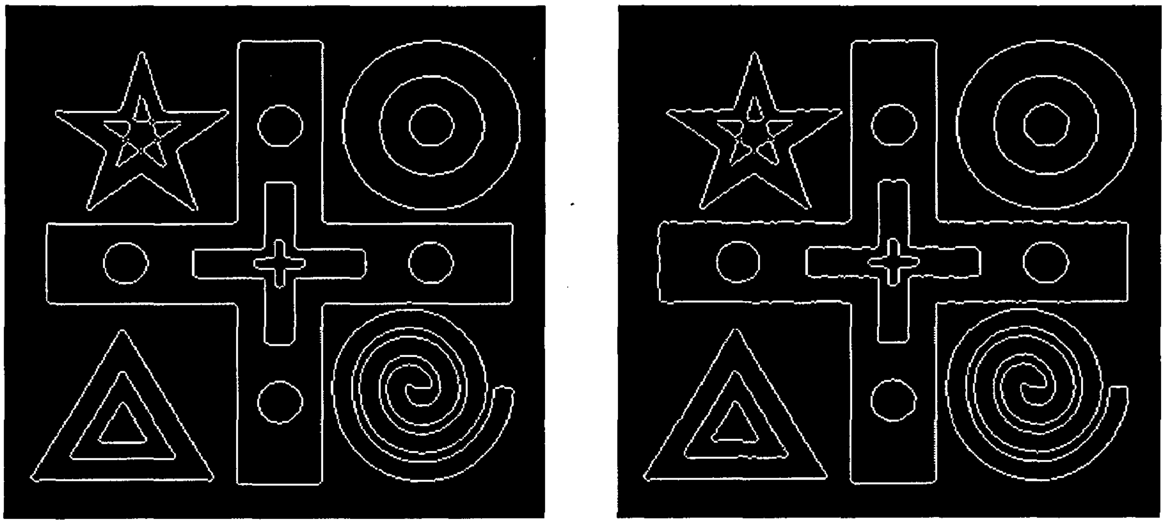

(a) (b)

Figure 4.5: Edge profile a) Original b) SRAD filtered

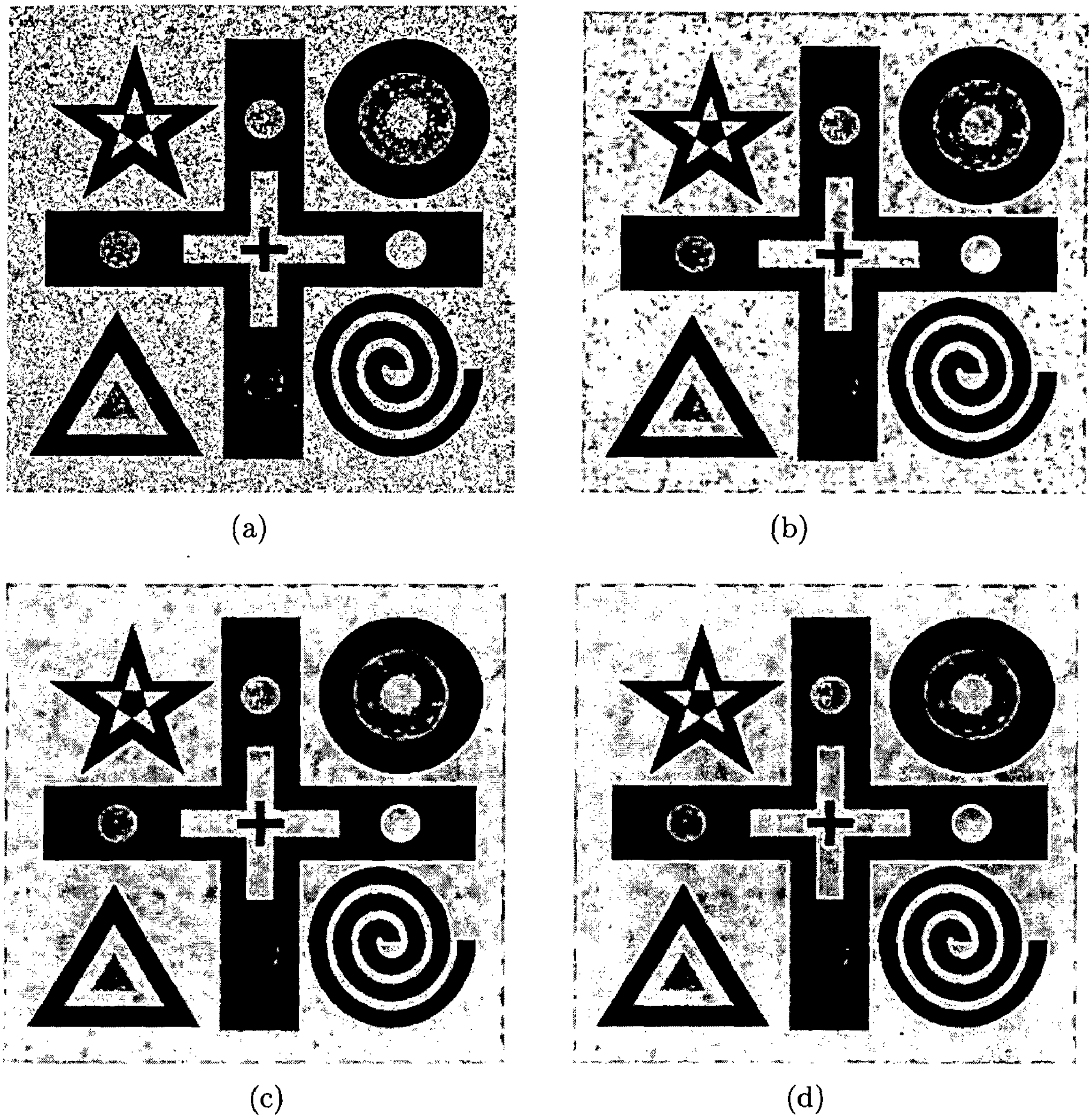

Figure 4.6: SRAD output for speckled distorted shape image after, (a) 20 iterations, (b) 100 iterations, (c) 220 iterations, (d) 300 iterations, t = 0.05

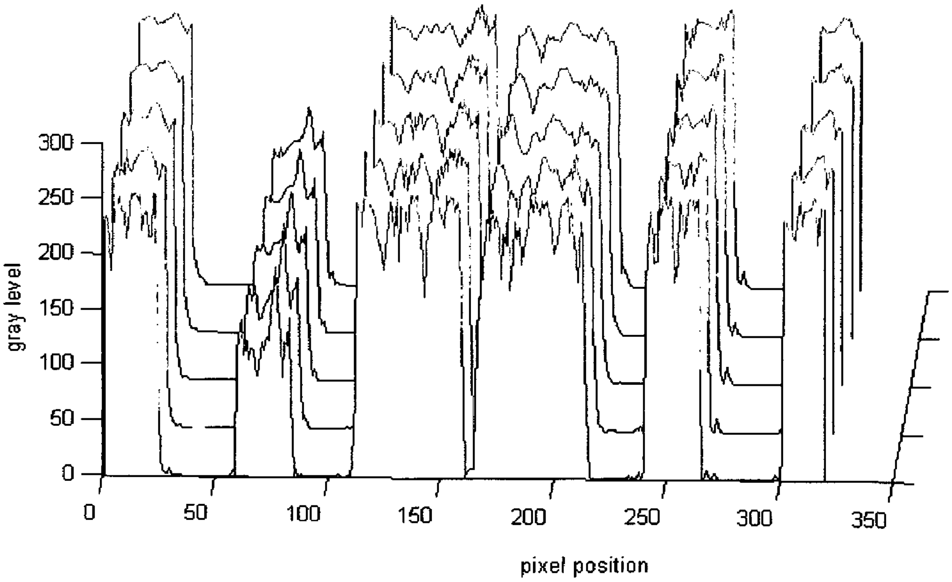

Figure 4.7: SRAD output profile for shape image along the line shown in Fig.4.4(b) for time step 0.05.

From the figure 4.7 , it is seen that as the no. of iterations increases the smoothining effect increases and after that the image may slightly become blurred due to the smearing of edges.

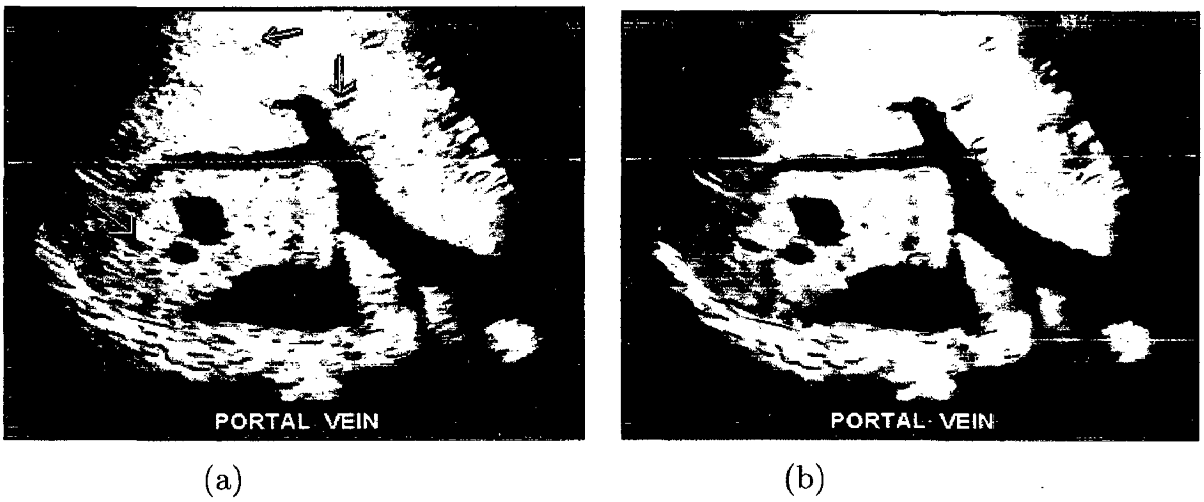

Figure 4.8: Portal vein image a) Original b) SRAD filtered

The SRAD algorithm is applied on the real ultrasound image of the portal vein as shown in fig 4.8, it is observed that the speckles have been reduced effectively in the filtered output. SRAD has also reatined the fine details marked with the arrow shown in fig 4.8(a) and also the cyst boundaries have been enhanced. This could be useful in auto segmentation and when the lesion boundaries are to be enhanced and delineated.

4.4 Conclusion

SRAD algorithm applied on both the simulated and the real ultrasound images gave a better visualization of the features masked by the speckle noise. Also SRAD removes the speckles effectively without causing blurring as compared to the adaptive filters. SRAD can also be used in the image segmentation and image registration.

Chapter 5

Results and Discussions

5.1 Introduction

In the previous chapters the adaptive filetrs and anisotropic diffusion filters were visually evaluated. To have a robust comparison , these methods should be evaluated quantitatively. In this chapter a quantiative comparison of the speckle reduction techniques(AWMF, ARGF, SRAD) has been done. For comparison of the performance: the ability to retain small details and edges i.e., sudden transitions in gray level or texture and gradual changes in gray level are taken as the yard sticks. Several quantitative measures like, figure of merit (FOM), contrast to noise ratio (CNR) and mean structural similarity index measure (MSSIM) have been calculated for this task. To achieve such evaluation, simulated images and ultrasound images of a "phantom", i.e., an artificial object with tissue-like acoustic properties have been used. The simulation and the phantom studies give quantitative performance analysis, while real ultrasound images were used to study the feasibility and usefulness of the methods. The real ultrasound images were shown to the radiologists to get the visual evaluation of the speckle reduction techniques. The details of the quantitative measures are depicted in subsequent section.

5.2 Evaluation Indices

Since speckle in the ultrasound image is modeled as the multiplicative noise, a linear image fidelity criterion, such as MSE or SNR, is not always an accurate measure of speckle suppression in images. In this work, the algorithm performance is quantified by using two quality indices: a noisy suppression quality index [24], an edge preservation index, called figure of merit (FOM) [25]. Speckle suppression is evaluated by comparing the structure similarity between denoised image and noise-free image.

5.2.1 Structural Similarity Test

Structural similarity index is used to compare the local patterns of pixel intensities that have been normalized for luminance and contrast [24]. Structural similarity index measure (SSIM) is defined as:

$$SSIM(x,y) = \frac{(2\mu_x\mu_y+C_1)(2\sigma_{xy}+C_2)}{(\mu_x^2+\mu_y^2+C_1)(\sigma_x^2+\sigma_y^2+C_2)}$$

where x and y are the image signal, which have been aligned with each other. μ_x and μ_y are the mean intensity for luminance comparison and σ_x and σ_y are standard deviation for contrast measurement. σ_{xy} is the correlation coefficient. C_i is the constant to avoid instability. All involved parameters were set as suggested in [24]. Mean SSIM (MSSIM) index is used for the overall quality measure of the entire image.

$$MSSIM(F,\hat{F}) = \frac{1}{M}\sum_{i=1}^{M} SSIM(x_i,y_i)$$

where F and $\hat{F}$ are the reference and the distorted images respectively. x_i and y_i are the image contents at the i^{th} local window and M is the number of windows.

5.2.2 Figure of Merit

To compare the edge preservation performance of the different filtering approaches, Pratt's FOM is used. The FOM is given by [25]:

$$FOM = \frac{1}{max\{\hat{N},N_{ideal}\}}\sum_{i=1}^{\hat{N}}\frac{1}{1+d_i^2\alpha}$$

where $\hat{N}$ and N_{ideal} are the number of detected and ideal edge pixels respectively, d_i is the Euclidean distance between i_{th} detected edge pixel and nearest ideal edge pixel and α is a constant typically set to 1/9. The FOM ranges between 0 and 1. A unity value of FOM stands for the ideal edge detection.

5.2.3 Contrast to Noise Ratio

The contrast-to-noise-ratio (CNR), which is sometimes referred as lesion signal-to-noise ratio [26] was computed by :

$$CNR = \frac{|\mu_1-\mu_2|}{\sqrt{\sigma_1^2+\sigma_2^2}}$$

where μ_1 and σ_1^2 are the mean and variance of intensities of pixels in a region of interest (ROI), and μ_2 and σ_2^2 are the mean and variance of intensities of pixels in a background region that has the same size as the ROI to be compared with.

5.3 Results

5.3.1 Results from Speckle Simulated Images :

The three speckle reduction techniques (AWMF, ARGF, SRAD) are applied on the shape image and Lena image, which are corrupted by speckle noise having a normal probability distribution function with mean = 0 and variance = 0.2. The original shape image and the speckle simulated image are shown in fig 5.1 Similarly lena image is depicted in fig 5.4(a) and speckle distorted is shown in fig 5.4(b). The filtered images by each of the techniques are shown in fig 5.5.

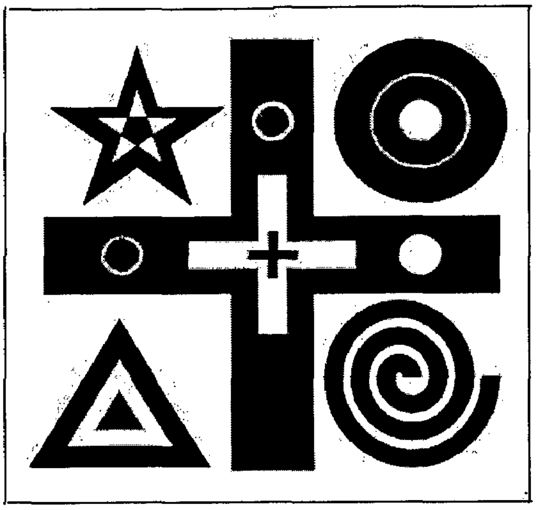

(a)

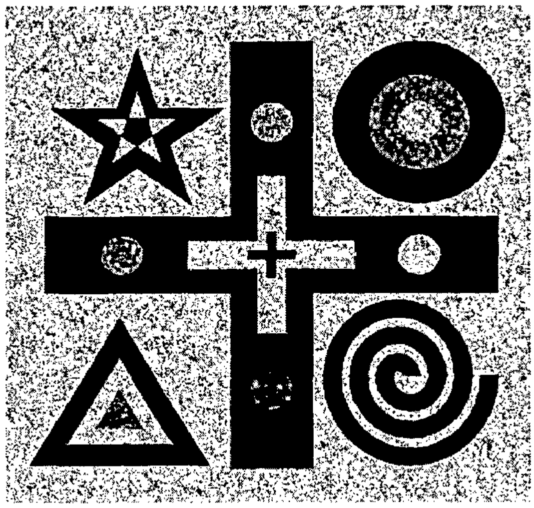

(b)

Figure 5.1: Shape image a) Original b) Simulated with speckle noise

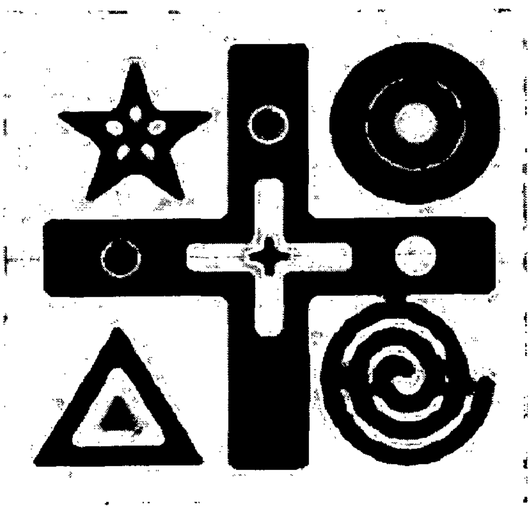

(a)

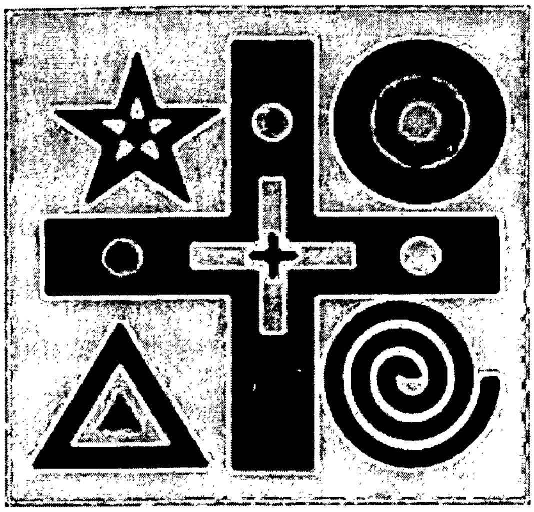

(b)

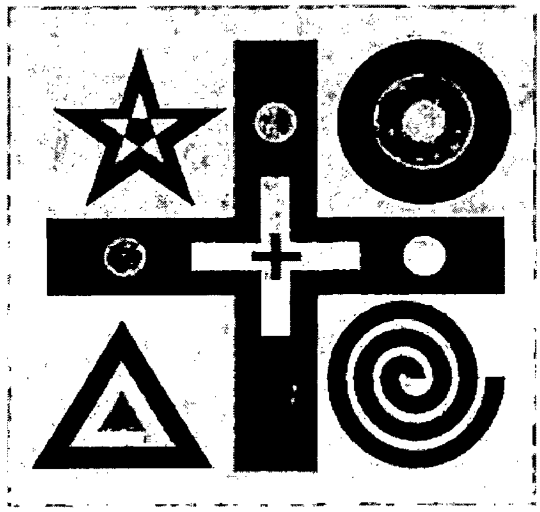

(c)

Figure 5.2: Filtered images a) AWMF filtered b) ARGF filtered c) SRAD filtered

From the filtered images it is clear that although AWMF reduces the speckles, it causes loss of details. ARGF suppresses the speckles while retaining the features, but it leads to smoothening of images. SRAD has been able to preserve the shape of different pattern in the shape image. Similar behaviour is observed for the simulated Lena image. To quantify the performance of each of the techniques the indices (FOM, MSSIM) are calculated. The resulted have been tabulated in table 5.1

Image	FOM	MSSIM
Noisy	0.453	0.560
AWMF	0.782	0.750
ARGF	0.852	0.780
SRAD	**0.898**	**0.810**

Table 5.1: FOM and MSSIM for shape image

For the filtered image to be close to the original image FOM and MSSIM should be close to 1. The higher value of FOM for SRAD shows that it is best at preserving the edges. High value of MSSIM indicates the filtered output from SRAD matches best with the original image. These figures indicate that SRAD is better than ARGF and AWMF at preservation of edges and reducing the speckles. ARGF causes smoothening of the image. Further from the edge profile of the original image and the filetred images shown in fig 5.3 it is clear that AWMF causes smearing and loss of sharp details. Similarly results were obtained for the Lena image and the results are tabulated in table 5.2.

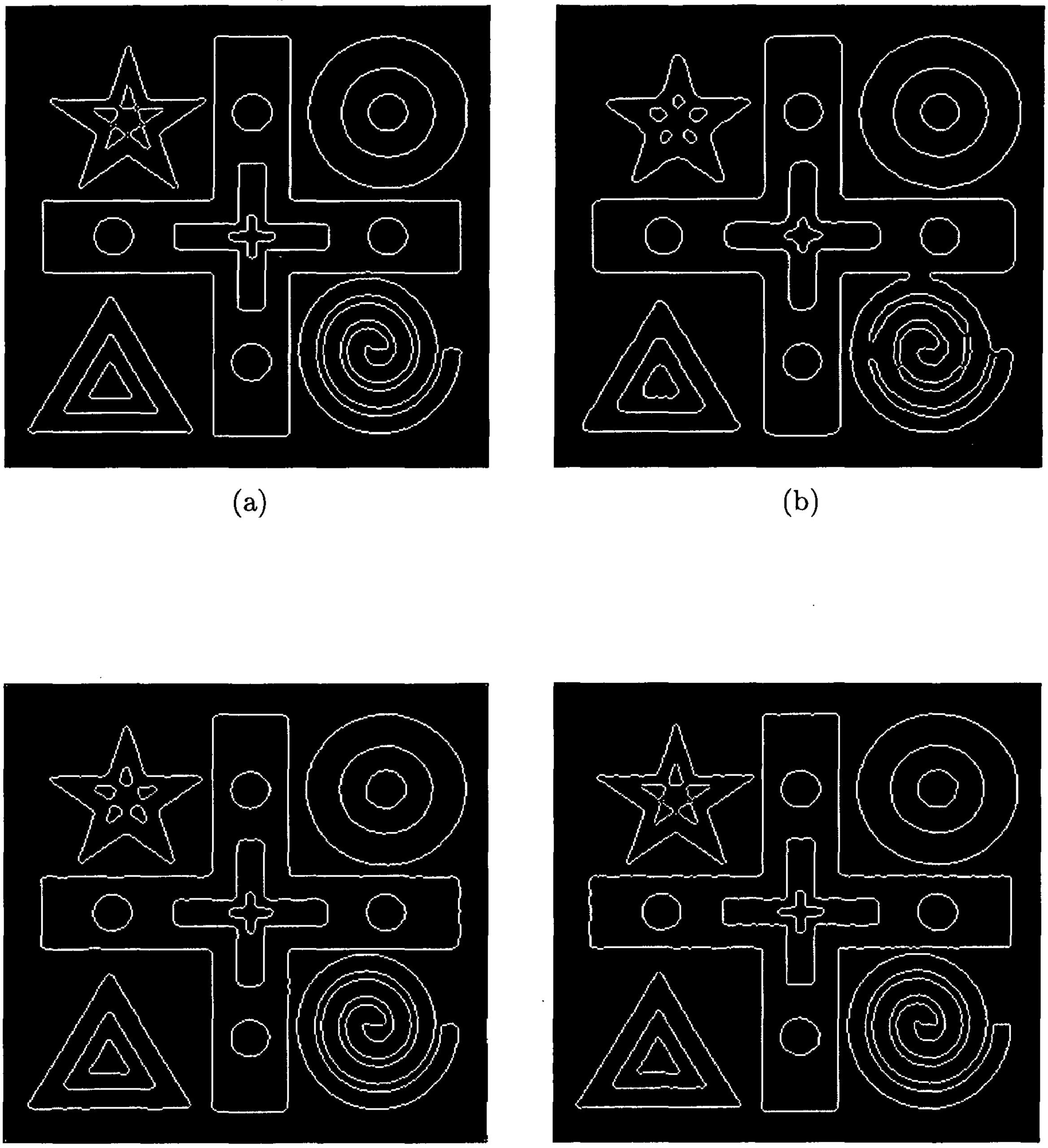

(a) (b) (c) (d)

Figure 5.3: Edge profile a) Original b) AWMF filtered c) ARGF filtered d) SRAD filtered

(a)

(b)

Figure 5.4: Lena image a) Original b) Simulated with speckle noise

(a)

(c)

(d)

Figure 5.5: Filtered images a) AWMF filtered b) ARGF filtered c) SRAD filtered

Image	FOM	MSSIM
Noisy	0.470	0.450
AWMF	0.570	0.640
ARGF	0.630	0.660
SRAD	**0.690**	**0.730**

Table 5.2: FOM and MSSIM for Lena image

Figure 5.6: Edge profile a) Original b) AWMF filtered c) ARGF filtered d) SRAD filtered

5.3.2 Results from Phantom Experiment

These three algorithm are applied on an ultrasound simulated cyst phantom image, shown in Fig. 5.7(a) to test their filtering efficiency and increasing the visualization. The cyst phantom consists of a collection of point targets, five cyst regions, and five highly scattering regions. This can be used for characterizing the contrast-lesion detection capabilities of a speckle redution technique. The cyst phantom image together with the filtered output is shown in fig 5.7. In the cyst image the ROI have been marked with numbers 1,2,3 to find their contrast to noise ratio (CNR) for each algorithm. The results have been shown in table 5.3. It is seen that for all the ROI' s (1,2,3) SRAD gave a higher value of CNR , thereby suggesting its ability in increasing the visualization of the organs and the small structures. SRAD outperforms the AWMF and ARGF filters at reducing the speckles and preserving the features.

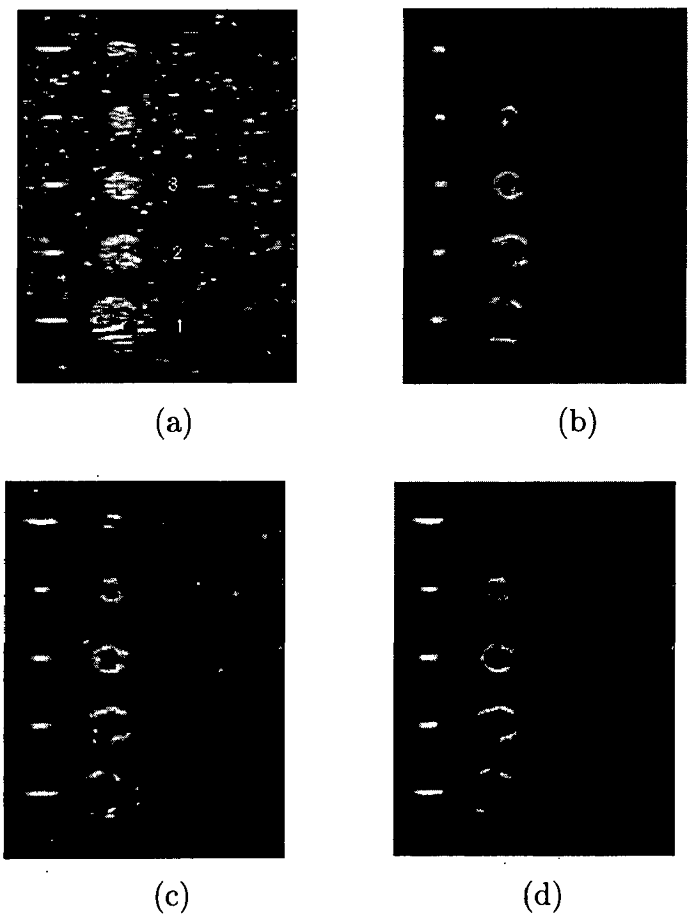

Figure 5.7: Speckle reduction output for phantom image: (a) Simulated with speckle noise, b) AWMF filtered c) ARGF filtered d) SRAD filtered

Image	ROI 1	ROI 2	ROI 3
Noisy	2.34	3.00	2.62
AWMF	5.22	5.47	4.41
ARGF	5.66	7.17	5.54
SRAD	**5.81**	**8.61**	**5.68**

Table 5.3: CNR values on a cyst phantom image

5.3.3 Result from Real Ultrasound

To test the filtering and the feature preservation ability , the three speckle speckle reduction techniques are applied on the clinical ultrasound images of Liver and portal vein. These images have different scales of information and should be useful to differentiate between the performances of the three techniques.

Case 1) Liver image

This case contains both large and small details. Results of this experiment are shown in fig 5.8. From the figure it is clear that SRAD has reduced the speckles effectively and the regions marked in circles have been preserved. The blood vessels region can be better visualized in SRAD filter image since speckle have been suppressed highlighting the boundary of the blood vessels. But these details have been lost in AWMF. ARGF filter has preserved the details but it has caused more smoothening as compared to SRAD.

The pixel values along the line 146 have been depicted in fig 5.9. To have clear view of the profile the pixel values from 100 to 280 have been shown separately in the fig 5.10. From this gray level profile it is clear that SRAD and ARGF are good at preserving the mean in homogenous region and variance in the area containing important features, while SRAD better than ARGF at reatining fine details.

ARGF smoothening ability can be used as a preprocessing step for auto segmentation and image registration.

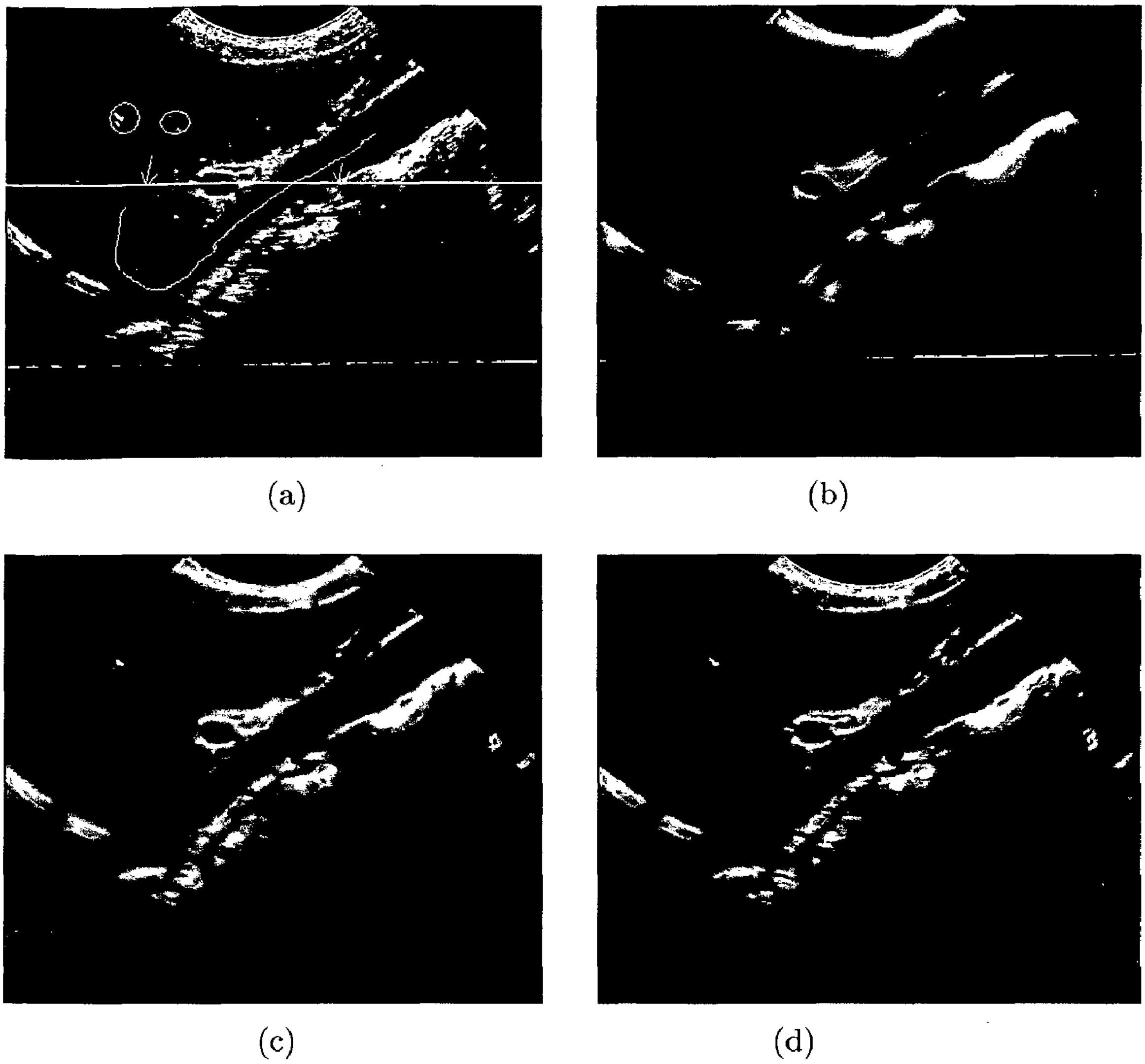

Figure 5.8: Results of ultrasound image of Liver a) Original b) AWMF c) ARGF d) SRAD

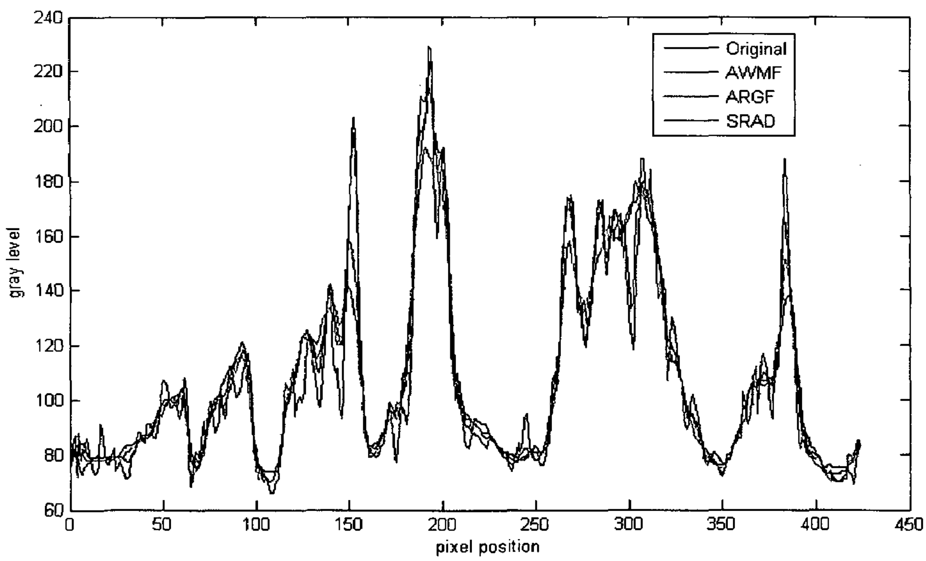

Figure 5.9: Profile along the line highlighted in liver image for three algorithms

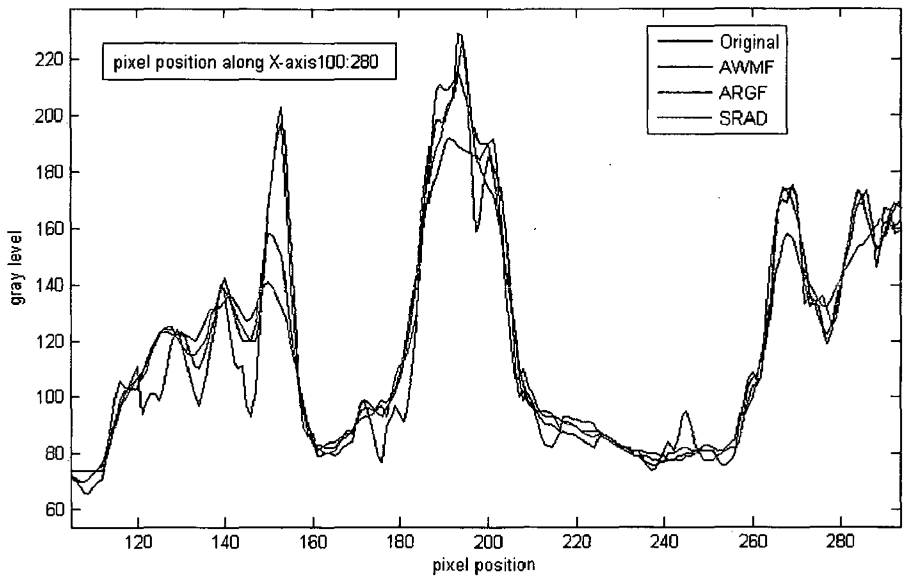

Figure 5.10: Profile along the pixel position 100 to 280

Case 2) Portal vein image

This image has cavities alongwith the important diagnostic features. The filtered images are shown in fig 5.11. If we compare the filtered images on the basis of retaining the texture and details, it is seen that AWMF blurs the details and speckles are not removed effectively. ARGF reduces the speckles but fine details are lost as compared to SRAD. The pixel profile along the line highlighted in the image supports this result.

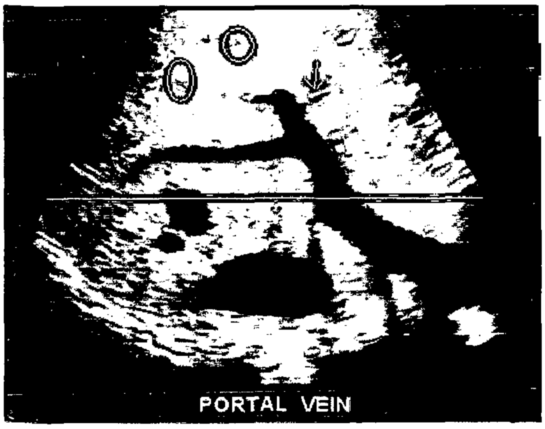

(a)

(b)

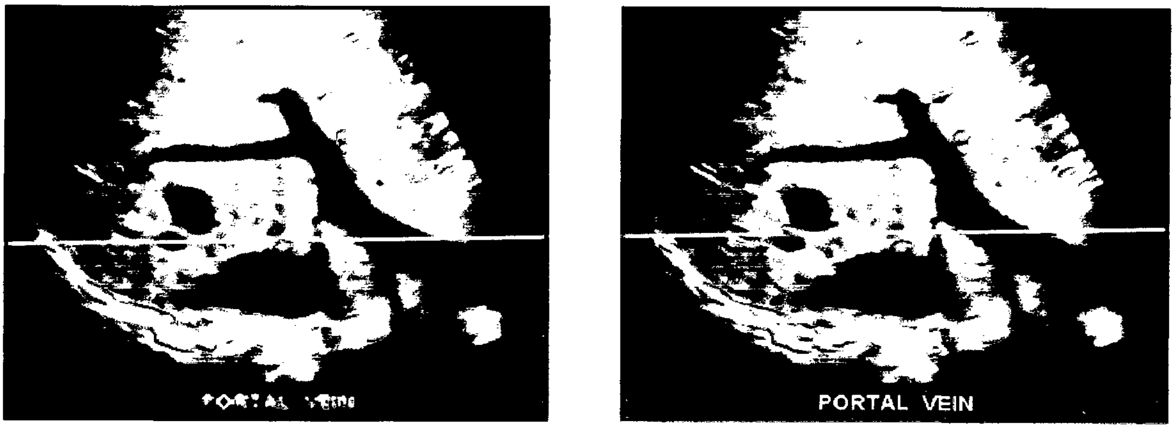

(c) (d)

Figure 5.11: Results of ultrasound image of Portal vein a) Original b) AWMF c) ARGF d) SRAD

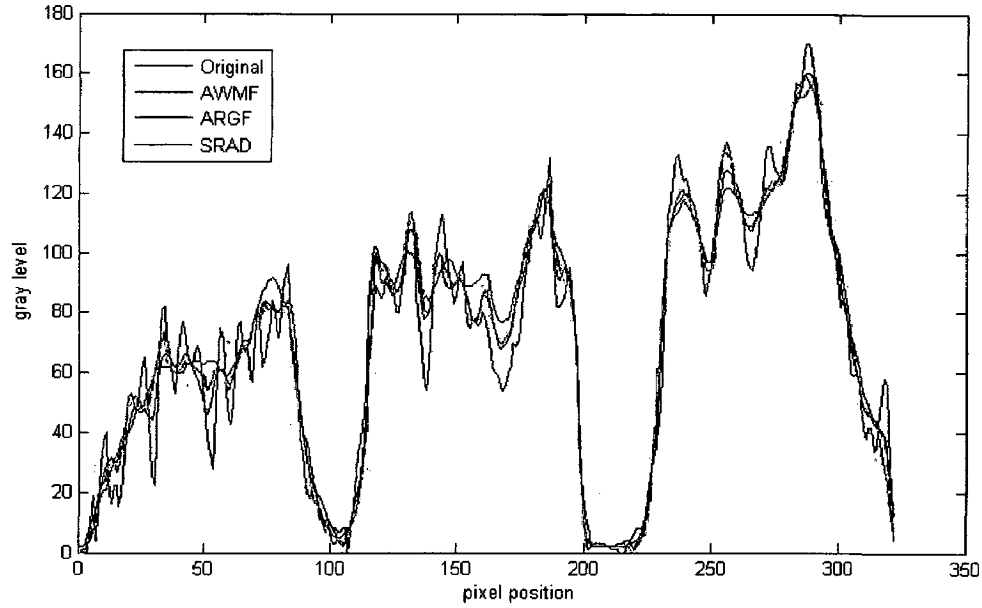

Figure 5.12: Profile along the line highlighted in portal vein image for three algorithms

If the compare ARGF and SRAD methods for the image simplification, for auto segmentation purpose it is observed that ARGF proves better than SRAD and hence can be used as a preprocessing step for image segmentation and image registration. Also it can help in diagnosis of the nature of lesion by delineating it's boundaries.

The portal vein image section with the cavities have been zoomed to show this nature of ARGF.

Figure 5.13: Image showing cavities a) ARGF b) SRAD

These algorithms were applied on four ultrasound B-scan images having different diagnostic features and information at different scales. From the results obtained, it was observed that the behaviour of these three techniques is same as seen above for the two cases. It was found that AWMF reduces the speckle but loss of diagnostic information occurs whereas in case of ARGF speckles were suppressed effectively, but very fine details were lost while filtering. SRAD improved the visualization of the structures while reducing the speckles. ARGF smoothening behaviour can be used for image simplification.

Chapter 6

Conclusion and Scope for Future Work

6.1 Conclusion

This thesis work introduced the speckle reduction techniques for the enhancement of the medical ultrasound images. The main objective of this thesis was to find out the best speckle reduction technique in terms of speckle reduction, feature preservation and as a preprocessing step for auto segmentation and image registration.

The work started with the introduction of a ultrasound imaging system and the speckle analysis incorporating various models developed to represent their statistics. The adaptive filtering and the diffusion based techniques were implemented for speckle suppression. Under the adaptive filtering the AWMF and ARGF were implemented and for the diffusion techniques SRAD was examined. To compare their performance, these algorithms were tested on the speckle simulated images and the tissue mimicking phantom. Then, the quantitative analysis was done to quantify the results obtained. The quantitative analysis was done using the indices FOM, MSSIM and CNR. SRAD gave the higher value for these indices when applied on a dataset of images. It can be concluded that for the better visualization and speckle reduction the SRAD technique outperforms the AWMF and ARGF techniques. But for auto segmentation and image registration, ARGF can be used as a preprocessing step.

Qualitaive analysis was done by presenting the filtered image to the radiologists. And it was found that technically speckle can be considered as a noise, but for a medical approach their texture should not be removed completely. And in this regard SRAD improves the visualization in medical ultrasound images.

6.2 Scope of the Future Work

The performance of ARGF method is highly dependent on the parameters obtained from the homogeniety model. Even these parameters vary from image to image. Therefore an independent estimation procedure for each new imaging configuration should be developed. The ARGF technique can be used for image simplification. The SRAD technique can be extended to three dimensions also. And a robust method can be developed to find the speckle scale function. Besides, the medical opinion in deciding the best algorithm should be considered.

Bibliography

[1] A. P. Dhawan, Y. Chitre, Kaiser-Bonassoand and M. Moskowitz,"Analysis of mammographic microcalcification using gray level image structure features," *IEEE Trans. Med. Imaging*, vol. 15, no. 3, pp. 246-259, 1996.

[2] Peter N. Burns,"Introduction to the physical principles of ultrasound imaging and doppler," *Fundamentals in Medical Biophysics*, November 2005.

[3] Brunner, Eberhard,"Ultrasound system consideration and their impact on front end components," *Analog Devices Inc.* 2002

[4] M. Karaman, M. A. Kutay and G. Bozdagi,"An adaptive speckle suppression filter for medical ultrasound imaging," *IEEE Trans. Med. Imaging*, vol. 14, no. 2, pp. 283-292, June 1995.

[5] P. C. Li and M. O'Donnell,"Elevational spatial compounding," *Ultrasound Imaging*, vol. 16, pp. 298-311, 1997.

[6] M. O'Donnell,"Optimum displacement for compound image generation in medical ultrasound," *IEEE Trans. Ultrasonics, Ferroelectric and Frequency Control*, vol. 35, pp. 470-476, 1988.

[7] T. Loupas, W. N. Mcdicken and P. L. Allan,"An adaptive weighted median filter for speckle suppression in medical ultrasound images," *IEEE Trans. Circuits and Systems*, vol. 36, no.1, pp. 129-135, 1989.

[8] J. I. Koo and S. B. Park,"Speckle reduction with edge preservation in medical ultrasonic images using a homogeneous region mean filter," *IEEE Trans. PAMI*, vol. 9, no. 5, pp. 690-698, 1987.

[9] Y.Chen, R. Yin, P. Flynn and S. Broschat,"Aggressive region growing for speckle reduction in ultrasound images," *Pattern Recognition Letters*, vol. 24, pp. 677-691, 2003.

[10] Y. Yu and S. T. Acton,"Speckle reduction anisotropic diffusion," *IEEE Trans. Image Processing*, vol. 11, no. 11, pp. 1260-1270, 2002.

[11] N. Nordstrom,"Biased anisotropic diffusion: a unified generalization and diffusion approach to edge detection," *Image Vision Comput.*, vol. 8, no. 4, pp. 318-327, 1990.

[12] P. Perona and J. Malik,"Scale space and edge detection using anisotropic diffusion," *IEEE Trans. Pattern Anal. Machine Intell.*, Vol. 12, no.7, pp. 629-639,1990.

[13] J. M. Thijssen,"Ultrasonic speckle formation, analysis and processing applied to tissue characterization," *Pattern Recognition Lettres*, vol. 24, pp. 659-675, 2003.

[14] R. F. Wagner, S. W. Smith, J. M. Sandrik and H. Lopez,"Statistics of speckle in ultrasound B-scans," *IEEE Trans. Sonics and Ultrasonics*, vol. 30, no. 3, pp. 156-163,1983.

[15] J. W. Goodman,"Some fundamental properties of speckles," *J. Opt. Soc. Am.*,vol. 66, no. 11,pp. 1145-1150 1976.

[16] E. Jackman,"On statistics of k-distributed noise," *Journal of Physics*, vol. 13, pp. 31-48, 1980.

[17] V. Dutt,"Statistical analysis off ultrasound echo envelope," Phd. Dissertation, Mayo Graduate School, Rochester, MN, 1995.

[18] D. T. Kaun, A. A. Sawchuk, T. C. Strand and P. Chavel," Adaptive restoration of images with speckle," *IEEE Trans. Acoustics., Speech and Signal Processing*, vol. 35, no. 3, pp. 373-382, 1987.

[19] J. S. Lee,"Digital image enhancement and noise filtering by using local statistics," *IEEE Trans. Pattern Anal. Machine Intell.*,vol. PAMI-2, pp. 165-168, 1980.

[20] D. T. Kaun, A. A. Sawchuk, T. C. Strand and P. Chave,"Adaptive noise smoothing filter for images with signal-dependent noise," *IEEE Trans. Pattern Anal. Machine Intell.*, vol. PAMI-7, no. 2, pp. 653-665, 1985.

[21] V. S. Frost, J. A. Stiles, K. S. Shanmugan and J. C. Holtzman,"A model for radar images and its application to adaptive digital filtering of multiplicative noise," *IEEE Trans. Pattern Anal. Machine Intell.*, vol. PAMI-4, no. 2, pp. 643-651, 1982.

[22] A. Lopes, R. Touzi and E. Nezry,"Adaptive speckle filters and scene heterogeneity," *IEEE Trans. Geoscience and Remote Sensing*, vol. 28, no. 6, pp. 992-1000, 1990.

[23] J. Weickert,"Anisotropic diffusion in image processing," Stuttgart, Germany: Teubner, 1998.

[24] Z. Wang, A. C. Bovik, H. R. Sheikh and E. P. Simoncelli," Image quality assessment: from error visibility to structure similarity," *IEEE Trans. on Image Processing,* vol. 13, no. 4, pp. 600-612, 2004.

[25] W. K. Pratt,"Digital image processing" New York: Wiley, 1977.

[26] Y. Chen, S. Broschat and P. Flynn,"Phase insensitive homomorphic image processing for speckle reduction," *Ultrason. Imaging*, vol. 18, no. 2, pp. 122-136, 1996.

[27] Y. Yu and S. T. Acton,"Edge detection in ultrasound imagery using the instataneous coefficient of variation," *IEEE Trans. Image Processing*, vol. 13, no. 12, pp. 1640-1655, 2004.